

Development of biomass derived highly porous fast adsorbents for post-combustion CO₂ capture

Sher, F., Iqbal, S. Z., Albazzaz, S., Ali, U., Mortari, D. A. & Rashid, T.

Author post-print (accepted) deposited by Coventry University's Repository

Original citation & hyperlink:

Sher, F, Iqbal, SZ, Albazzaz, S, Ali, U, Mortari, DA & Rashid, T 2020, 'Development of biomass derived highly porous fast adsorbents for post-combustion CO₂ capture', Fuel, vol. 282, 118506.

<https://dx.doi.org/10.1016/j.fuel.2020.118506>

DOI 10.1016/j.fuel.2020.118506

ISSN 0016-2361

Publisher: Elsevier

NOTICE: this is the author's version of a work that was accepted for publication in Fuel . Changes resulting from the publishing process, such as peer review, editing, corrections, structural formatting, and other quality control mechanisms may not be reflected in this document. Changes may have been made to this work since it was submitted for publication. A definitive version was subsequently published in Fuel, 282 (2020) DOI: 10.1016/j.fuel.2020.118506

© 2020, Elsevier. Licensed under the Creative Commons Attribution-NonCommercial-NoDerivatives 4.0 International <http://creativecommons.org/licenses/by-nc-nd/4.0/>

Copyright © and Moral Rights are retained by the author(s) and/ or other copyright owners. A copy can be downloaded for personal non-commercial research or study, without prior permission or charge. This item cannot be reproduced or quoted extensively from without first obtaining permission in writing from the copyright holder(s). The content must not be changed in any way or sold commercially in any format or medium without the formal permission of the copyright holders.

This document is the author's post-print version, incorporating any revisions agreed during the peer-review process. Some differences between the published version and this version may remain and you are advised to consult the published version if you wish to cite from it.

Development of biomass derived highly porous fast adsorbents for post-combustion CO₂ capture

Farooq Sher^{a,*}, Sania Zafar Iqbal^b, Shaima Albazzaz^{c,d}, Usman Ali^e, Daniela Andresa Mortari^f, Tazien Rashid^{g,h}

a. School of Mechanical, Aerospace and Automotive Engineering, Faculty of Engineering, Environmental and Computing, Coventry University, Coventry CV1 2JH, UK

b. Department of Biochemistry, University of Agriculture, Faisalabad 38000, Pakistan

c. Department of Chemical and Environmental Engineering, University of Nottingham, University Park, Nottingham NG7 2RD, UK

d. Department of Chemical Engineering, College of Engineering, University of Basrah, Basrah, Iraq

e. Department of Chemical Engineering, University of Engineering and Technology, Lahore 54890, Pakistan

f. São Carlos School of Engineering, University of São Paulo (USP), São Carlos, SP, Brazil

g. Department of Chemical Engineering, NFC Institute of Engineering and Fertilizer Research Faisalabad, Pakistan

h. Department of Chemical Engineering, Universiti Teknologi Petronas, Bandar Seri Iskandar, Tronoh 32610, Perak, Malaysia

*Corresponding author:

Dr Farooq Sher

Lecturer

School of Mechanical, Aerospace and Automotive Engineering

Faculty of Engineering, Environmental and Computing

Coventry University

Coventry

CV1 2JH

UK

E-mail address: Farooq.Sher@coventry.ac.uk (F.Sher)

Tel.: +44 (0) 24 7765 7754

40 **Abstract**

41
42 This study is carried out for a comparative screening of three groups of biomasses; soft or non-
43 woody (peanut shell); intermediate woody (walnut shell) and hard woody (pine wood) for the
44 development of adsorbents/activated carbons for post-combustion CO₂ capture (over N₂
45 balance). Three different groups of biomass residues are selected to study the role and nature
46 of the material in adsorption and selection of the raw material for CO₂ adsorbents synthesis for
47 future researches because of the hot issue of anthropogenic CO₂ emissions. The adsorption
48 isotherms studied by the thermal gravimetric analyser (TGA) revealed that CO₂ adsorption
49 capabilities are in the range of 2.53–3.92 mmol/g (over N₂ balance) at 25 °C. The newly
50 synthesised activated carbons (ACs) exhibited a fast rate of adsorption as 41–94% in the initial
51 2 minutes. Porous surface development with catalytic KOH activation is seen clearly through
52 SEM surface morphological analyses and mathematically confirmed from S_{BET} ranges from
53 146.86 to 944.05 m²/g. FTIR and XRD peaks verify the generation of basic or inorganic O₂-
54 rich moieties that help in acidic CO₂ capture. It has also been observed from adsorption
55 isotherms that the order of higher adsorption groups is as; peanut shell > pine wood > walnut
56 shell, while the best activation mass ratio (sample/KOH) is 1:3. The synthesised low cost ACs
57 with an amount of 1.93 US\$ per kg production could help to overcome the environmental
58 hazards and problems caused by CO₂ and biomass waste.

59
60 **Keywords:** CO₂ capture; Biomass waste; Green activated carbons; Adsorption; KOH-
61 activation; Microporous materials and Global warming.

62

63 **1 Introduction**

64 Because of the human activities, there is a noticeable increase observed in the warming of
65 earth's atmosphere and expected to continue throughout the present century as of industrial
66 development. This rapid progress of modern civilization is the primary cause of CO₂ emissions

67 to the environment. Anthropogenic CO₂ from greenhouse gases is a main contributor to the
68 global warming that is mostly discharged from fossil fuels combustion. Currently, the use of
69 fossil fuels as an energy source continues to increase especially in developing countries, this is
70 due to the availability of fossil fuels at a reasonable cost [1, 2]. Literature confirmed the
71 increment of > 30 billion tons of CO₂ to the atmosphere per year [3]. CO₂ emissions with this
72 rate has upraised numerous alarms including urban smog, health issues as well as acid rain.
73 Therefore, it is an urgent need of the hour to stabilise the level of this anthropogenic greenhouse
74 pollutant (CO₂) before the extensive destruction. Consequently, in the presence of continuous
75 climate change, the European Commission has decided to lessen its carbon discharge by 20–
76 95% between 2020–2050 with reference to 1990 levels [4]. It is cleared in present energy setups
77 of fossil fuels consumption, that the implementation of CO₂ capture and its storage (CCS)
78 technologies could display an essential role to achieve the necessary reduction in CO₂
79 emissions to avoid irreversible and eternal destruction to the atmosphere [5-7].

80

81 At present, total three technologies have been introduced for CCS: pre-combustion capture,
82 post-combustion capture and oxy-fuel combustion process. Post-combustion CSS technology
83 can be simply retrofitted to the present-day power stations, petrochemical and gas industries,
84 oil refineries and cement industries which worldwide accounts for nearly half of the CO₂
85 emissions [8, 9]. Various separation techniques are available for post-combustion capture
86 which includes absorption, cryogenic separation, adsorption and membrane [10, 11]. The
87 physical technique proved to be effective for the separation and purification of gas is
88 adsorption. In adsorption technique, the solid sorbents used for capturing CO₂ have potential
89 advantages over other conventional capturing treatment techniques including greater capacity,
90 ease of handling, selectivity and reduced energy for regeneration.

91

92 However, adsorption method is costly, therefore, utilizing cheap materials for adsorbent
93 preparation makes the method worthwhile. These materials include forestry wastes,
94 agricultural residues and sewage sludge, the first two precursors have more carbon and very
95 less ash content [12]. Different fruit stones, the by-products collected from food processing
96 units are special concern for obtaining carbon adsorbents with a better regular porous surface
97 and appreciable hardness. Peach stones, apricot stones [13], olive stones [14], cherry stones
98 [15] and grapestones [16] have been used as raw materials for the fabrication of activated
99 adsorbents with high porosity and surface areas. Coconut shells have also been used for the
100 fabrication of microporous adsorbents [17].

101

102 Activation of biomass is achieved by two methods; chemical activation and physical activation.
103 The chemical activation method has some benefits over physical activation method. Firstly, it
104 is a single step carbonization followed by activation with an activating agent and secondly, it
105 is performed at a lower temperature as compared to physical activation [18]. The chemical
106 activation procedure is associated with precursor material impregnation with activating agents
107 (NaOH, KOH, ZnCl₂ or salts) then carbonized under inert pressure and finally washed to
108 remove chemicals so that porous structure is left behind. Carbon adsorbents have been used for
109 the treatment of industrial wastewater, removal of organic and inorganic pollutants from flue
110 gases. In addition to its applications, the activated carbon is used as an adsorbent for CO₂
111 removal [12]. CO₂ adsorbents had been prepared from different starting materials other than
112 biomass-based residues and by-products. A group of researchers prepared CO₂ adsorbents by
113 KOH activation of petroleum pitch precursor [19]. The fabricated material exhibited an
114 outstanding adsorption potential for CO₂ with values as high as 380 mg CO₂ /g sorbent at 0 °C
115 temperature and 1 bar pressure. Nitrogen enriched CO₂ adsorbents have also been prepared
116 from formaldehyde-urea resin by chemical activation with KOH [20]. For these nitrogen

117 enriched activated carbons (ACs), the CO₂ adsorption limit is 1.40 mmol/g at 30 °C temperature
118 under 12.5% CO₂ flow. Recently, a study is carried out to analyse the effects of CO₂ adsorption
119 by ACs in terms of power loss and thermal efficiency. Upon comparison, it is concluded that
120 ACs are more advantageous than the commercial adsorbents in rappings of cost and efficiency
121 [21].

122

123 In the present study, different groups of biomass residues have been selected to study the role
124 and nature of material in post-combustion CO₂ adsorption. The ACs have been prepared using
125 biomass residues, therefore, this synthesis could be helpful in reducing landfill space to
126 overcome the pollution and environmental issues caused by CO₂ emissions. The importance
127 of this study over others is the diverse nature of biomass residues and their activation with a
128 wide range of catalytic KOH. This research has identifies that which activation ratio is
129 important in each group that is helpful for developing interesting surface chemistry, consistent
130 morphology and porous surface structure with excellent surface parameters. The calculation of
131 cost estimation for the production of per kg of ACs has also been performed, in order to verify
132 the cheapness of these adsorbents.

133

134 **2 Experimental**

135 Total twelve ACs have been prepared. The thermal gravimetric analyser (TGA) was used to
136 study the CO₂ adsorption (over N₂ balance) of synthesised ACs. TGA results helped in the
137 selection of the best samples from each group for further testing.

138 **2.1 Synthesis of activated carbons**

139 Biomass product; pine wood (PW) and by-products; peanut shell (PN) and walnut shell (NS)
140 were selected as materials for the preparation of ACs. Pine wood was produced in Pakistan
141 while the other two biomasses were obtained from a local market in the United Kingdom. First

142 raw materials (PW, PS and WS) were crushed, then sieved to a particles of size of 1 mm for
143 further treatment. Potassium hydroxide (KOH) with 99% concentration (conc.) used as an
144 activating agent was purchased from Sigma-Aldrich.

145
146 Biomass-based activated carbons (ACs) were prepared using a single-step chemical activation
147 process, which can successfully develop potassium moieties on raw materials. In this protocol,
148 3 grams of prepared raw material (PW, PN and NS) samples were first mixed physically with
149 KOH (99% conc.) at different mass ratios including; 1:1, 1:2, 1:3 and 1:4 of raw sample/ KOH
150 (m/m). The physically mixed mixture (raw sample/KOH) was then heated in a horizontal tube
151 furnace. The activation was carried out at 750 °C temperature with 5 °C/min heating rate in the
152 presence of 1 L/min nitrogen flow [4].

153
154 When the reaction was reached at to a specific temperature, the mixture was kept at this
155 temperature for 1 hour, before it was cool down in nitrogen (N₂) to ambient conditions. All the
156 times, the neutral gas (N₂) was flowing inside the reaction furnace at 1 L/min flow rate. To get
157 final products of ACs mixtures were removed from the furnace and cool down to room
158 temperature then washed until neutral with distilled water (usually 3 times washing through
159 200 mL of water). The twelve synthesised activated carbons were labelled according to their
160 precursor and mass ratio of activation agent are shown in Table 1.

161

162 **2.2 CO₂ adsorption**

163 CO₂ capture/adsorption measurements of ACs samples were carried out using
164 thermogravimetric analysis (TGA Q500, TA Instruments USA). For individual measurements
165 of CO₂ uptake, the sample was first dried at 120 °C in the presence of neutral N₂ gas for 1/2
166 hour to eliminate any possible physisorbed CO₂ and/or the moisture content. Then the

167 temperature was lowered to 25 °C for adsorption and stabilized. The reaction environment
168 inside the reaction sample chamber was switched to flue gas (15% CO₂ in N₂) from N₂ at 100
169 mL/min flow rate at the above set adsorption's temperature for 1 hour. The weight of final
170 sample was noted to estimate the CO₂ uptake. CO₂ adsorption measurements were performed
171 to analyze the ACs/adsorbents' surface affinity for CO₂ [22].

172

173 **2.3 Characterisation**

174 Ultimate analysis of the biomass samples was performed using a Flash EA 1112 elemental
175 analyzer. Proximate analysis was obtained using the same TGA Q-500 instrument by heating
176 the sample (s) from 10 to 110 °C/min in N₂ flow rate. These conditions were maintained for 10
177 minutes to obtain the moisture content. The temperature was then increased from 110 to 700
178 °C at 20 °C/min flow rate (under N₂) and kept for 30 minutes at these conditions to get the
179 weight loss due to devolatilisation after this temperature was ramped at the same rate to 950
180 °C/min. The reaction environment was then switched from N₂ to air, inside the furnace
181 compartment and kept it isothermal for 40 minutes to oxidise the char completely to obtain the
182 fixed carbon and ash contents [23]. The results of different weight percentages of fixed carbon
183 (FC), ash, volatile matter (VM), carbon (C), nitrogen (N), hydrogen (H) and oxygen (O) of raw
184 precursors (PN, NS, and PW) are presented in Table 2.

185

186 Micromeritics ASAP 2420 instrument was used for surface textural parameter measurements
187 of the prepared ACs with N₂ uptake of the ACs at 77 K. The ACs were degassed first at 120
188 °C temperature for 16 hours before micromeritics measurements. The specific surface area
189 (S_{BET}) was calculated by standard Brunauer–Emmett–Teller (BET) method utilising the N₂
190 isotherm adsorption data within 0.01 to 0.1 relative pressure range. The adsorbed quantities of

191 N₂ at P/P₀ of ca. 0.99 were used for the calculation of total or cumulative pore volumes (V_{total}).
192 Average pore diameter was determined using $4V_{total}/S_{BET}$ [24].

193

194 The volume of micropore (V_{micro}), was estimated by t-plot method. Total mesopore volume
195 V_{meso} obtained by subtracting the micropore volume from the total pore volume [25]. Then the
196 micro porosity percentage of the selected ACs was calculated by V_{micro}/V_{total} . Similarly, the
197 mesoporosity percentage was calculated using V_{meso}/V_{total} . Crystallographic analyses of the
198 synthesised carbons before and after activation were inspected with the help of D8 Advance
199 XRD diffractometer (Bruker Inc., Germany) and Cu K α radiation source. While the values of
200 voltage and current used for XRD experiments were 40 kV and 40 mA respectively.

201

202 Organic moieties generated on the surface of ACs were characterised by Fourier Transform
203 Infrared (FTIR) Spectroscopy (Bruker Vertex 70 spectrometer) [26]. For FTIR investigations
204 sample pellets were prepared with potassium bromide salt. The spectras were noted in between
205 400–4000 cm⁻¹ wave number range. A mortar was used to ground 0.0015 g sample with 0.25 g
206 of KBr. The obtained powder was then placed under a mechanical pressure of 10 kPa/mm² in
207 a circular die for 10 seconds. After this, the sample was transferred to an oven for drying at 100
208 °C for 48 hours under vacuum to avoid any interface between the mix, CO₂ molecules and
209 water vapours. The temperature was reduced to room temperature under vacuum overnight. At
210 the last, the sample was transferred to the analyser.

211

212 Surface morphology of all the raw samples as well as the best performing ACs derived from
213 these samples were obtained by using a scanning electron microscope (SEM) instrument (JEOL
214 7100F FEG-SEM) at 15 kV. Between three and four repeat runs for each experiment were
215 performed to ensure appropriate repeatability and validity of the results.

216

217 **3 Results and discussion**

218 **3.1 Evaluation of CO₂ capture performance**

219 The CO₂ adsorption (over N₂ balance) isotherms of twelve fabricated ACs (Table 1) are plotted
220 in Fig. 1 to Fig. 3. Adsorption kinetics were determined from TGA as a function of time at 25
221 °C temperature. These CO₂ adsorption isotherms shown a remarkable CO₂ uptake capacity of
222 ACs ranging from 2.53 to 3.92 mmol/g. While the lower range of CO₂ (over N₂ balance) uptake
223 (2.53 mmol/g) of this study is comparable to other ACs synthesised from phenolic resins [27]
224 and rice husk waste [4]. The phenolic resin based carbons were activated with different ratio
225 of HNO₃ while rice husk carbons were activated with different KOH ratio. In both of these
226 previous studies, CO₂ adsorption was not more than 2 mmol/g. The synthesised ACs derived
227 from three different biomass precursors (NS, PN and PW), each biomass sample was reacted
228 with four different ratios of KOH. Therefore, four different ACs (NSK1, NSK2, NSK3 and
229 NSK4) were synthesised from walnut shell biomass only. Treatment with KOH changes the
230 textural properties and chemical nature of functional groups of precursors. Activation with
231 different mass ratios of KOH strategy was applied in to prepare K-ACs with high porosity,
232 surface area and increased amount of basic oxygen functionality, all these factors helped in
233 higher CO₂ uptake. This activation strategy with different KOH ratios was also proved to be
234 beneficial from previous researches [28]. Higher amount of KOH helps in the generation of
235 more porous structures followed by high CO₂ uptakes, this can be confirmed from Fig. 1, as
236 different KOH amount yields different CO₂ uptake these results are in accordance with Singh,
237 G., et al., [28].

238

239 The CO₂ uptake of 3.23>2.90>2.71>2.57 mmol/g were noted for walnut shell derived different
240 ACs NSK3>NSK4>NSK1>NSK2 respectively as shown in Fig. 1. These values are reported

241 by rounding off the digits up to two decimal places. Similarly, 3.92>3.18>3.06>2.54 and
242 3.49>3.24>2.84>2.53 mmol/g uptakes were measured for peanut shell samples:
243 PNK3>PNK1>PNK2>PNK4 (Fig. 2), and pine wood samples: PWK1>PWK2>PWK3>PWK4
244 (Fig. 3) respectively. The best activated carbon from the walnut shell is NSK3, from peanut
245 shell is PNK3 and from pine wood biomass is PWK1.

246

247 Comparatively, from three groups, the most highly activated carbon is PNK3 and least one is
248 PWK4. In the case of walnut shell ACs, 3.23 mmol/g of CO₂ adsorption peak was noticed,
249 while the overall CO₂ adsorption is 60% in initial 4 minutes after that it was increased
250 constantly with time for 1h. Similar trends were noticed for other carbons in the same time
251 interval. Up to 16 minutes NSK4 showed a higher rate of uptake, but after that NSK3 exhibited
252 a sudden increase in CO₂ uptake and goes on increasing up to 60 minutes. The CO₂ uptake
253 capacity of different walnut shell ACs is different and increased little by increasing the mass
254 ratio of KOH (KOH/sample) up to 3:1. Beyond this combination, further increase in the amount
255 of activating agent did not increase the CO₂ uptake of the activated carbon (Fig. 1). For NSK4
256 the CO₂ uptake is lowered to some extent as compared to NSK3 that could be because of the
257 lower number of adsorption, active and suitable functional group sites.

258

259 For peanut shell derived ACs, 3.92 mmol/g CO₂ adsorption peak was noticed while the overall
260 CO₂ adsorption is equivalent to 80% in initial 3 to 4 minutes. After this initial 80% adsorption
261 capacity, horizontal plateaus of adsorption isotherms were observed for PNK1 and PNK2
262 indicating the saturation of available microspores (Fig. 2). A constant increase of adsorption
263 with time was observed for PNK3 also illustrates from its blue isotherm (Fig. 2). However, for
264 PNK4 a decrease in adsorption capacity was observed that was similar to NSK4 isotherm.
265 Likewise, for pine wood derived ACs, the peak value of 3.49 mmol/g for CO₂ adsorption was

266 observed. The overall CO₂ adsorption is equivalent to 91% in initial 2 to 3 min followed by
267 somewhat horizontal plateaus of adsorption for PWK1 and PWK2 [4]. While for PWK3 and
268 PWK4 relatively lower adsorptions were noticed that could be because of a decrease in porosity
269 with an increase in KOH activation (Fig. 3).

270

271 Physisorption carbons with porous surfaces have reasonably fast kinetics [29]; comprise
272 diffusional transports in micro and macropores. That's why this study is designed on the
273 physisorption principle (CO₂ uptake). All these CO₂ adsorption kinetics results in association
274 with different KOH mass ratios concluded that the best group for that has shown fast CO₂
275 uptake rates is PW derived ACs, while the group for higher CO₂ adsorption capacity is PN
276 derived ACs (Fig. 4). The adsorption amount reported with TGA is CO₂ adsorption over N₂
277 balance rather than pure CO₂ adsorption [4], because flue gas comprises of 15% CO₂ with N₂
278 [30]. It is observed that CO₂ adsorption capacities of ACs are higher than N₂ but in parallel N₂
279 adsorbs little with CO₂ in flue gas analysis. While the amount of N₂ is reported usually less or
280 equals to 0.5 mmol/g [31].

281 **3.2 Textural analysis of activated carbons**

282 N₂ adsorptions were performed for six samples (Fig. 5) out of twelve among which three were
283 those exhibited higher CO₂ uptake (PNK3>PWK1>NSK3). The other three selected ACs were
284 those either the least adsorbed carbon (PNK4) from a particular group of ACs with higher KOH
285 ratio or the carbon with relatively higher CO₂ uptake but with least ratio of KOH (NSK1) from
286 another group of ACs. The effect of porosity on the adsorption of N₂ is shown in the form of
287 N₂ adsorption isotherms. Surface textural and pore structure calculations obtained from the
288 BET measurements are incorporated in Table 3. It can be seen that V_{total} and S_{BET} increased
289 from 0.07 to 0.38 cm³/g and 112.33 to 944.05 m²/g respectively for different ACs fabricated at

290 750 °C and 0.15 bar pressure. It is cleared that the ACs derived from KOH activation protocol
291 are microporous with the microporosity accounting for up to 95% of the total porosity.

292

293 The N₂ sorption (adsorption and desorption) isotherms of PNK3, PWK1, PNK4, NSK1 and
294 PWK2 are found similar to Type I isotherm that is also verified from the International Union
295 of Pure and Applied Chemistry (IUPAC) data sources [32]. While one of the selected samples,
296 NSK3 has shown Type II isotherm. Literature confirms that N₂ sorption Type I isotherms are
297 obtained for those adsorbents having very small pores usually known as micropores. The
298 presence of these micropores verifies from sharp N₂ uptake capacity of PNK3, PWK1, PWK2
299 and NSK1 adsorbents at low pressure <0.1 bar. Afterwards, the development of horizontal
300 plateaus at higher pressures attributed to an extraordinary microporosity of these selected ACs
301 ranges from 72 to 95%. These results provide the reasons for higher CO₂ uptake and fast
302 adsorption kinetics of the above mentioned ACs. Comparatively at further higher pressures,
303 variable minor to significant hysteresis loops are observed for PWK1, NSK3, PNK4, PWK2
304 and NSK1. Hysteresis loop suggests the presence of mesoporous surface of adsorbent at these
305 pressures generated by the gas condensation [22]. While Type II N₂ adsorption isotherm shown
306 by the adsorbent NSK3 indicates mesoporous surface with 15% microporosity.

307

308 Higher specific surface area and micropores volume of PNK3, higher adsorption capacities of
309 NSK3 and PWK1 derived ACs support the variable amount strategy of KOH used for
310 activation from minor (1:1) to significant (1:4) range is successful. Increase in micropores
311 volume and surface area is detected because of oxidation and gasification reactions proceed via
312 decomposition of potassium carbonate (K₂CO₃) at a high temperature that is also supported
313 with SEM images.

314

315 The lower S_{BET} of two selected ACs; NSK3>PNK4 is 146.86>112.33 m²/g. This decreasing
316 order of S_{BET} is observed with an increasing ratio (1:3 to 1:4) of the activating agent in the
317 synthesised ACs. This might be because of the over oxidation of carbons and development of
318 insoluble potassium (K) residues. The relatively lower S_{BET} obtained for activated carbons was
319 because of K impregnation that led to fractional or even thorough occlusion of pores.
320 Therefore, a peak concentration of potassium is observed, above that the additional residual
321 potassium (PNK4) helps little to capture CO₂. This discussion confirms that the overall best
322 ratio among all 12 fabricated ACs derived from three different groups of precursors is 1:3
323 (sample: KOH) because on further activation with KOH leads to over oxidation and formed
324 macro-pores credited to adsorption of 2.54 mmol/g of CO₂ uptake. From Table 3, it could be
325 verified that the BET measurements for these adsorbents are consistent with their Type I (Fig.
326 5f) and Type II (Fig. 5e) isotherms [33]. Fig. S1 shows an observed comparative analysis of
327 N₂ adsorbed volumes of the selected ACs. Furthermore, it is seen that the volume of N₂-
328 adsorbed for PNK4 is very small owing to its relatively lower developed total pores V_{total} .

329
330 The presence of different pore sizes in selected ACs from each group are comparatively
331 illustrated in Fig. 6. In the case of PNK3, PWK1 and PWK2 three different pore sizes have
332 been generated; micropores/mesopores (< 50 nm) and macropores (> 50 nm). While in the case
333 of NSK1, NSK3 and PNK4 the most probably generated pores are < 50 nm in size. Among
334 these, more are mesopores (2–50 nm) while some are micropores (< 2 nm). Fig. S2 investigates
335 the bimodal pore structure and its development by KOH activation of the best performing ACs
336 from different groups. Fig. S3 shows an observed dependence of CO₂ uptake on the developed
337 pore volume by KOH treatment.

338

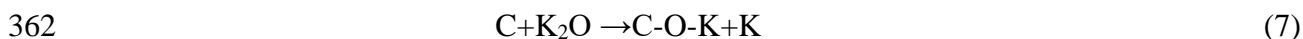
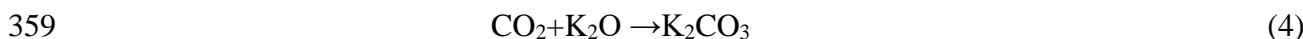
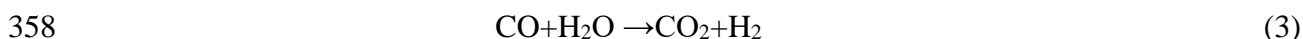
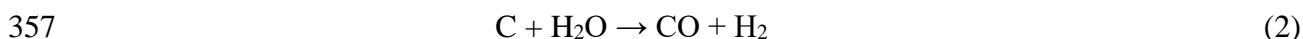
339 3.3 KOH intercalation mechanism

340 Type I isotherms Fig. 5(a-d, f) are observed because KOH impregnation acts as a catalyst to
341 speed up the gasification reaction as mentioned in equations (2, 3, 5 and 6) [32, 34]. Reaction
342 intermediates, K_2CO_3 and K_2O are formed at a temperature >700 °C. These polar/basic
343 intermediates react with the carbon matrix to fabricate a framework with micropores. The
344 carbon framework development from non-porous to porous upon treatment with KOH is also
345 confirmed by SEM analyses.

346

347 Polymeric components present in biomass undergo different chemical reactions including
348 cracking, aromatisation, dehydration, dehydrogenation and depolymerisation during
349 carbonisation process followed by treatment with KOH base [28]. The later reaction is applied
350 to activate the carbon matrix through a series of reactions (1 to 8). The redox reaction of
351 biomass carbon with KOH leads to oxidation of carbon matrix that yields potassium carbonate
352 (K_2CO_3) and hydrogen (H_2) gas (reactions 2 to 4). The oxidation process and resultantly the
353 presence of oxidised species on the surface of ACs are in agreement with relevant FTIR peaks
354 in the developed oxidised functional group region ($1000-1860\text{ cm}^{-1}$).

355



364

365 Progressively, as temperature arose the chemicals/functional groups of biomass decompose
366 and gasification occurs (reactions 5, 6 and 8), rest of the mass forms char through aromatisation
367 reaction. The presence of aromatic groups after activation is observed from the FTIR peaks of
368 activated carbons in the related fingerprint region (808–893 cm^{-1}). Gasification/ or escape of
369 volatile components cause the development of porous surface from non-porous carbon
370 framework/matrix [20].

371

372 The biomass carbon reacts with the KOH until it is consumed completely and as a result
373 converted into metallic K and other volatiles. K_2CO_3 formed, further reacts with carbon
374 (biomass) to generate K_2O , K and volatiles reactions (4 to 8). The development of high porosity
375 is credited to the (reactions 2 to 8) of dehydration, polymerisation and evolution of gases.
376 Potassium based compounds formed (reaction 7) during the activation process are well
377 intercalated/ or impregnated into the carbon framework. While later the removal of these
378 compounds (K species) using water treatment results in the fabrication of porous surfaces of
379 ACs [32]. Therefore, it can be said that the possible effect of KOH treatment on the studied
380 carbons was porosity generation with well observed gasification reactions.

381

382 **3.4 Crystalline surface analysis**

383 The synthesised CO_2 adsorbents have also been studied for their microcrystalline or amorphous
384 nature by powdered XRD patterns (Fig. 7). These analyses were applied to a selected number
385 of activated (NSK1, NSK3, PNK3, PNK4, PWK1 and PWK2) and corresponding non-
386 activated carbons (NS, PN and PW) to identify the changes on the surface of adsorbents before
387 and after activation. The peak intensities in the case of activated carbons and non-activated
388 carbons are in exact accordance with the KOH ratios. In case of all non-activated and some

389 activated carbons, one broad and two weak peaks have been noticed around $2\theta = 22\text{--}25^\circ$, 43°
390 and 45° . A broad peak of quite high intensity around $22\text{--}25^\circ$ is observed for NS, PN and PW
391 carbons that confirms the amorphous nature of non-activated carbons. This peak around 22--
392 25° is identical to (002) diffraction of graphite and confirms the hexagonal nature of NS, PN
393 and PW carbons. While the two weak peaks around $2\theta = 43^\circ$ and 45° corresponded to the (101)
394 and (100) diffraction planes of graphite are observed in relation to their partial microcrystalline
395 nature [4].

396

397 A clear shift in XRD peaks has been observed for activated carbons in comparison to non-
398 activated carbons of all groups. In case of walnut shell derived activated carbon NSK1
399 relatively less intense peaks are detected around 25° , 43° and 45° . The peak (002) diffraction
400 plane of graphite is absent in case of NSK3 in comparison to raw non-activated carbon NS.
401 The absence of this characteristic peak might be due to the collapse of carbon matrix. The
402 encircled area sharp peaks of NSK3 may be attributed to the development of more chemical
403 species in the interlayers of collapse hexagonal graphite (carbon). Likewise, in the case of
404 peanut shell derived ACs, again interesting surface chemistry has been confirmed from XRD
405 patterns. Broad peaks around the characteristic range of $22\text{--}25^\circ$ and 43° in the case of non-
406 activated PN are developed into sharp ones for PNK3 because of increasing KOH ratio. It is
407 also observed from XRD pattern that sample/KOH ratio of 1:4 is not helpful in the activation
408 of carbons because in the case of PNK4, the peaks almost disappeared in comparison to PNK3
409 and PN. The intensity of the observed peaks is also lowered in comparison to 1:3 and 1:2 ratios.
410 This type of behaviour might be noted as of destructive interferences developed because of a
411 relatively high amount of KOH [20]. This destructive interference of KOH might cause the
412 degradation of porous structures. Moreover, XRD profiles of pine wood groups are exactly

413 similar to the peanut shell group. The peak centred around 26° to 27° is noticed for the
414 generation of inorganic crystalline compounds [35].

415

416 **3.5 Surface chemistry analysis**

417 FTIR analyses were performed for six samples. Three were non-activated carbons: NS, PN and
418 PW and three activated carbons: NSK3, PNK3 and PWK1. In the case of walnut shell based
419 non-activated carbon NS; the presence of peaks at 3664 (O-H str), 3263 (N-H str), 2467 (O-H
420 str), 1857 (C=O str), 1660 (C=O str), 1463, 1326 (O-H def) and 690 (CH def) cm^{-1} correspond
421 to OH, NH or might be chelate, carboxylic acid, carbonyl group of quinone, α - β unsaturated
422 ketone, methyl, alcohol and alkenyl groups respectively (Fig. 8). However, NSK3 spectra
423 confirms its activation and graphitisation that is also verified with the similar results obtained
424 from XRD profiles of this material. The peaks of NSK3 at 3664 (O-H str), 3263 (N-H str),
425 2397, 1774 (C=O str), 1620 (C=O str), 1458 (C=C), 1344 (O-H def), 1120 (C-O str), 808 (CH
426 def) and 617 (CH def) cm^{-1} indicate the generation of OH, NH/ or might be chelate, carboxylic
427 acid, ester, carbonyl group with benzene, double bond of aromatic ring, alcohol, ether, *p*-
428 substituted aromatic ring and alkenyl groups respectively (Fig. 8). Like in NSK3, almost
429 similar type of functional groups were developed on the surface of PNK3 after activation that
430 might be because of the same mass ratio of the activating agent.

431

432 The presence of peaks at 3691 (O-H str), 2891 (CH str), 2380, 1832 (C=O), 1645 (C=O str),
433 1450 (def), 1249 (C-O str) and 640 (def) cm^{-1} correspond to OH, aldehyde, carboxylic acid,
434 carbonyl of anhydride, carbonyl of diaryl ketone, methyl, diaryl ether and CH groups
435 respectively in the case of PN non-activated carbon (Fig. 9). This precursor on activation with
436 KOH in 1:3 ratio fabricated PNK3, its FTIR spectra confirms its activation. Furthermore, these
437 FTIR results are also supported with SEM results of the respective AC. The peaks of PNK3 at

438 3514 (O-H str), 2437, 1853 (C=O str), 1714 (C=O str), 1575 (N-H def), 1398 (O-H def), 1002
439 (C-O str), 873 (CH def) and 723 (rocking ν) cm^{-1} correspond to dimer or chelate, carboxylic
440 acid, carbonyl of anhydride, carbonyl of diaryl ketone, aromatic amine, phenol, ether,
441 substituted aromatic ring and CH groups respectively (Fig. 9).

442

443 Likewise, for PW precursor the bands at 2314, 1799 (C=O str), 1672 (C=O str), 1471 (def) and
444 779 (CH def) cm^{-1} correspond to carboxylic acid, carbonyl of acid halide, carbonyl of diaryl
445 ketone, CH₃, *m*-disubstituted aromatic group, while PWK1 with 1:1 KOH/sample ratio
446 indicated bands at 3683 (O-H str), 2351, 2250 (str), 1814 (C=O), 1635 (N-H def), 1469, 1315
447 (C-O), 1112 (C-O str), 893, 798 and 657 cm^{-1} attribute to free OH, carboxylic acid, alkenyl,
448 carbonyl of acid halide, secondary amine, alcohol, C-O of anhydride, ether, two bands for weak
449 and strong *m*-disubstituted aromatic ring and CH groups respectively (Fig. 10). The presence
450 of dimers, chelates and disubstituted aromatic ring in the case of PNK3, NSK3 and PWK1,
451 confirms the aromatisation reactions with KOH impregnation. The developed basic groups of
452 ACs help in the adsorption of acidic CO₂ because of electrostatic interactions developed
453 between them at a higher temperature (reaction 7).

454 **3.6 Surface morphology analysis**

455 The morphological analyses were carried out for non-activated (NS, PN and PW) precursors
456 and the best performed ACs including; NSK3 from NS, PNK3 from PN and PWK1 from PW.
457 These ACs not only showed higher CO₂ uptake in their groups but also confirmed with FTIR
458 spectra, their modified surface chemistries in comparison to their non-activated forms as a
459 result of activation. Walnut shell based non-activated precursors NS shows non-porous and flat
460 morphology in comparison to their activated form NSK3 as illustrated in (Fig. 11). SEM
461 images of NSK3, clearly show changed surface morphology than precursor not showing more

462 microspores. Additionally, the pore diameter of NSK3 is seen much larger than other porous
463 ACs; PNK3 (Fig. 12d) and PWK1 (Fig. 13b).

464

465 Moreover, it could reasonably be said that the decomposition of carbon matrix/walls of NSK3
466 connecting porous structure via high content of KOH took place. Carbon walls oxidised at high
467 temperature 750 °C, generated K residues that change its morphology completely. Therefore,
468 it could be concluded that NSK3 revealed a carbon matrix collapse with a higher mass ratio of
469 KOH. Sometimes, if the higher CO₂ capture of activated carbons (K-ACs) cannot be
470 compatible with surface textural features then porosity decreases with activation. Then in such
471 cases, the higher CO₂ uptake of K-ACs attributes to modified surface chemistries [28]. In the
472 case of NSK3 potassium intercalation instead of relatively lower microporosity plays a key role
473 in CO₂ capacities. Therefore, it could be said that the polarized surface functional groups are
474 helpful to enhance surface interaction with quadrupole moment of CO₂ and consequently
475 instigated higher CO₂ uptake [28].

476

477 The SEM images of non-activated peanut shell derived precursor PN showed a flat non-porous
478 surface and developed into a highly porous surface (PNK3) on treatment with an activating
479 agent as illustrated in Fig. 12. Removal of gases during the process of activation according to
480 redox stoichiometric equations ((5) to (6) and (8)) were credited to a flat, regular and 87%
481 microporosity of PNK3 [20]. These pores justify more diffusion/ or adsorption of CO₂ from
482 bulk to the adsorbent (PNK3) surface. Porosity generation phenomenon was also observed
483 similar to the peanut shell in pine wood group. There is a clear difference between the
484 morphological surfaces of PW, PWK1, non-activated and activated forms of pine wood
485 precursor and carbon respectively as shown in Fig. 13.

486 **3.7 Fast adsorption potential**

487 CO₂ adsorption (over N₂ balance) measurements for the first 120 seconds have been reported
488 for activated carbons. The CO₂ uptake measurements of adsorbents in the first 120 seconds in
489 comparison to 1 hour verified that the developed ACs are very responsive and free from time
490 dependent factor to much extent. From Table 4, it could be observed that almost all adsorbents
491 with one or two exceptions showed an average >60% uptake of CO₂ from total in the first 120
492 seconds. In the case of walnut shell derived ACs (Fig. S4(a)) the CO₂ uptake in first 120 sec is
493 50% in average, which is 20% lower than peanut shell derived ACs (Fig. S4(b)) and 30% lower
494 than pine wood derived ACs (Fig. S4(c)). The possible reason behind this could be the different
495 composition and diverse nature of the material. Moreover, PNK2 and PWK2 have presented
496 an ideal case by adsorbing more than 90% of CO₂ from the total in first 120 seconds. Under
497 the current scenario of environmental pollution [36, 37], there is a need to develop renewable
498 fuels [38] and sustainable technologies [39, 40] to reduce CO₂ emissions and control global
499 warming [41]. Hence, biomass based carbon adsorbents are excellent renewable materials that
500 could be used to capture CO₂ from coal fired power plants.

501

502 **3.8 Cost estimation**

503 From cost estimation analysis with respect to per kg production, it is observed that the
504 synthesised ACs are cheaper and comparable to the others commercially available. An amount
505 of 1.93 US\$ is calculated for the production of per kg of AC as shown in Table 5, while the
506 amount of commercially available AC is in the range of 2–5 US\$ per kg [42]. In literature, the
507 synthesised ACs from the peels of *Artocarpus integer* fruit following the steam activation
508 method were estimated to be cost-effective adsorbents (1.67 US\$ per kg) [42], but these
509 carbons were not evaluated for their CO₂ uptake potentials. Furthermore, the cost estimation

510 analysis was carried out by following the summation of sample per kg cost of different
511 components [42].

512 **4 Conclusions**

513 Detailed screening and development of adsorbents/ACs from diverse biomass residues that are
514 cheap, low cost, sustainable, green agricultural waste, easily available and CO₂ neutral
515 materials is carried out. This synthesis of ACs from biomass precursors will not only overcome
516 the global warming issue but would also minimise the problems of land space covered by the
517 selected biomass residues.

- 518 • TGA and BET analyses demonstrate that the adsorption capacities of different ACs are
519 as; 3.23>2.90>2.71>2.57, 3.92>3.18>3.06>2.54 and 3.49>3.24>2.84>2.53 mmol/g for
520 NSK3>NSK4>NSK1>NSK2, PNK3>PNK1>PNK2>PNK4 and
521 PWK1>PWK2>PWK3>PWK4 respectively. Among all these the highest CO₂ (3.92
522 mmol/g) is noticed with PNK3 AC that is peanut shell derived.
- 523 • N₂ adsorption isotherms show Type I isotherm for NSK1, PNK3, PNK4, PWK1 and
524 PWK2 and Type II isotherm for NSK3.
- 525 • Bimodal pore structure analyses verify the Type I and Type II N₂ sorption isotherms
526 results.
- 527 • Peaks in the region < 50 nm confirm that mostly adsorbents' surface comprised of micro
528 and mesopores.
- 529 • The catalytic KOH mechanistic approach and the resultant aromatization and
530 gasification reactions are in accordance with FTIR peaks in region (808–893 cm⁻¹) and
531 verified from SEM images.
- 532 • Characteristic XRD peaks of 2θ = 22-25° and 43° in case of non-activated precursors
533 are developed into sharp ones for ACs.

- 534 • Cost estimation calculation showed the developed ACs are cheaper in comparison to
535 commercially available ones.
- 536 • Future research could be directed towards soft woody biomass residues because they
537 yield relatively more porous adsorbents upon activation with KOH than hard woody
538 biomass.

539 **Acknowledgement**

540 The authors are thankful to the Higher Education Commission of Pakistan for the financial
541 support to carry on this research.

542

543 References

- 544 1. Li, J., et al., Selective preparation of biomass-derived porous carbon with controllable
545 pore sizes toward highly efficient CO₂ capture. *Chemical Engineering Journal*, 2019.
546 360: p. 250-259.
- 547 2. Sher, F., et al., Thermal and kinetic analysis of diverse biomass fuels under different
548 reaction environment: A way forward to renewable energy sources. *Energy Conversion*
549 *and Management*, 2020. 203: p. 112266.
- 550 3. Li, B., et al., Advances in CO₂ capture technology: A patent review. *Applied Energy*,
551 2013. 102: p. 1439-1447.
- 552 4. Liu, X., et al., Potassium and zeolitic structure modified ultra-microporous adsorbent
553 materials from a renewable feedstock with favorable surface chemistry for CO₂ capture.
554 *ACS applied materials & interfaces*, 2017. 9(32): p. 26826-26839.
- 555 5. Sher, F., et al., Oxy-fuel combustion study of biomass fuels in a 20 kW th fluidized bed
556 combustor. *Fuel*, 2018. 215: p. 778-786.
- 557 6. Sher, F., et al., Experimental investigation of woody and non-woody biomass
558 combustion in a bubbling fluidised bed combustor focusing on gaseous emissions and
559 temperature profiles. *Energy*, 2017. 141: p. 2069-2080.
- 560 7. Hai, I.U., et al., Experimental investigation of tar arresting techniques and their
561 evaluation for product syngas cleaning from bubbling fluidized bed gasifier. 2019. 240:
562 p. 118239.
- 563 8. Figueroa, J.D., et al., Advances in CO₂ capture technology—The US Department of
564 Energy's Carbon Sequestration Program. *International Journal of Greenhouse Gas*
565 *Control*, 2008. 2(1): p. 9-20.
- 566 9. Coninck, H.d., et al., IPCC special report on carbon dioxide capture and storage.
567 Intergovernmental Panel on Climate Change, 2005.
- 568 10. Wang, M., et al., Post-combustion CO₂ capture with chemical absorption: a state-of-
569 the-art review. *Chemical Engineering Research and Design*, 2011. 89(9): p. 1609-1624.
- 570 11. Hai, I.U., et al., Assessment of biomass energy potential for SRC willow woodchips in
571 a pilot scale bubbling fluidized bed gasifier. 2019. 258: p. 116143.
- 572 12. Ao, W., et al., Microwave assisted preparation of activated carbon from biomass: A
573 review. *Renewable and Sustainable Energy Reviews*, 2018. 92: p. 958-979.
- 574 13. Djilani, C., et al., Adsorption of dyes on activated carbon prepared from apricot stones
575 and commercial activated carbon. *Journal of the Taiwan Institute of Chemical*
576 *Engineers*, 2015. 53: p. 112-121.
- 577 14. Hazzaa, R. and M. Hussein, Adsorption of cationic dye from aqueous solution onto
578 activated carbon prepared from olive stones. *Environmental Technology & Innovation*,
579 2015. 4: p. 36-51.
- 580 15. Nowicki, P., J. Kazmierczak, and R. Pietrzak, Comparison of physicochemical and
581 sorption properties of activated carbons prepared by physical and chemical activation
582 of cherry stones. *Powder Technology*, 2015. 269: p. 312-319.
- 583 16. Jimenez-Cordero, D., et al., Preparation of granular activated carbons from grape seeds
584 by cycles of liquid phase oxidation and thermal desorption. *Fuel Processing*
585 *Technology*, 2014. 118: p. 148-155.
- 586 17. Ello, A.S., et al., Coconut shell-based microporous carbons for CO₂ capture.
587 *Microporous and Mesoporous Materials*, 2013. 180: p. 280-283.
- 588 18. Tay, T., S. Ucar, and S. Karagöz, Preparation and characterization of activated carbon
589 from waste biomass. *Journal of Hazardous Materials*, 2009. 165(1-3): p. 481-485.

- 590 19. Wahby, A., et al., High-surface-area carbon molecular sieves for selective CO₂
591 adsorption. *ChemSusChem*, 2010. 3(8): p. 974-981.
- 592 20. Tiwari, D., H. Bhunia, and P.K. Bajpai, Adsorption of CO₂ on KOH activated, N-
593 enriched carbon derived from urea formaldehyde resin: kinetics, isotherm and
594 thermodynamic studies. *Applied Surface Science*, 2018. 439: p. 760-771.
- 595 21. Jiang, L., et al., Post-combustion CO₂ capture from a natural gas combined cycle power
596 plant using activated carbon adsorption. *Applied Energy*, 2019. 245: p. 1-15.
- 597 22. Liu, J., et al., Spherical potassium intercalated activated carbon beads for pulverised
598 fuel CO₂ post-combustion capture. *Carbon*, 2015. 94: p. 243-255.
- 599 23. Sait, H.H., et al., Pyrolysis and combustion kinetics of date palm biomass using
600 thermogravimetric analysis. *Bioresource Technology*, 2012. 118: p. 382-389.
- 601 24. Lin, G., et al., KOH activation of biomass-derived nitrogen-doped carbons for
602 supercapacitor and electrocatalytic oxygen reduction. *Electrochimica Acta*, 2018. 261:
603 p. 49-57.
- 604 25. Hirst, E., A. Taylor, and R. Mokaya, A simple flash carbonization route for conversion
605 of biomass to porous carbons with high CO₂ storage capacity. *Journal of Materials
606 Chemistry A*, 2018.
- 607 26. Yakout, S. and G.S. El-Deen, Characterization of activated carbon prepared by
608 phosphoric acid activation of olive stones. *Arabian Journal of Chemistry*, 2016. 9: p.
609 S1155-S1162.
- 610 27. Sun, N., et al., Surface-modified spherical activated carbon materials for pre-
611 combustion carbon dioxide capture. *RSC Advances*, 2015. 5(42): p. 33681-33690.
- 612 28. Singh, G., et al., Single step synthesis of activated bio-carbons with a high surface area
613 and their excellent CO₂ adsorption capacity. *Carbon*, 2017. 116: p. 448-455.
- 614 29. Presser, V., et al., Effect of pore size on carbon dioxide sorption by carbide derived
615 carbon. *Energy & Environmental Science*, 2011. 4(8): p. 3059-3066.
- 616 30. Rashidi, N.A. and S. Yusup, An overview of activated carbons utilization for the post-
617 combustion carbon dioxide capture. *Journal of CO₂ utilization*, 2016. 13: p. 1-16.
- 618 31. Li, M. and R. Xiao, Preparation of a dual pore structure activated carbon from rice husk
619 char as an adsorbent for CO₂ capture. *Fuel processing technology*, 2019. 186: p. 35-39.
- 620 32. Liu, X., et al., Developing hierarchically ultra-micro/mesoporous biocarbons for highly
621 selective carbon dioxide adsorption. *Chemical Engineering Journal*, 2019. 361: p. 199-
622 208.
- 623 33. Güleç, F., F. Sher, and A. Karaduman, Catalytic performance of Cu-and Zr-modified
624 beta zeolite catalysts in the methylation of 2-methylnaphthalene. *Petroleum Science*,
625 2019. 16(1): p. 161-172.
- 626 34. Wang, J. and S. Kaskel, KOH activation of carbon-based materials for energy storage.
627 *Journal of Materials Chemistry*, 2012. 22(45): p. 23710-23725.
- 628 35. Wang, K., et al., Promising biomass-based activated carbons derived from willow
629 catkins for high performance supercapacitors. *Electrochimica Acta*, 2015. 166: p. 1-11.
- 630 36. Cuce, E., et al., Strategies for ideal indoor environments towards low/zero carbon
631 buildings through a biomimetic approach. *International Journal of Ambient Energy*,
632 2019. 40(1): p. 86-95.
- 633 37. Zhang, Y., et al., Simulation of Particle Mixing and Separation in Multi-Component
634 Fluidized Bed Using Eulerian-Eulerian Method: A Review. *International Journal of
635 Chemical Reactor Engineering*, 2019. 17(11).
- 636 38. Al-Juboori, O., et al., The effect of variable operating parameters for hydrocarbon fuel
637 formation from CO₂ by molten salts electrolysis. *Journal of CO₂ Utilization*, 2020. 40:
638 p. 101193.

- 639 39. Al-Shara, N.K., et al., Electrochemical study of different membrane materials for the
640 fabrication of stable, reproducible and reusable reference electrode. *Journal of Energy*
641 *Chemistry*, 2020. 49: p. 33-41.
- 642 40. Cuce, E., et al., Sustainable ventilation strategies in buildings: CFD research.
643 *Sustainable Energy Technologies and Assessments*, 2019. 36: p. 100540.
- 644 41. Hassan, M.H.A., et al., Kinetic and thermodynamic evaluation of effective combined
645 promoters for CO₂ hydrate formation. *Journal of Natural Gas Science and Engineering*,
646 2020: p. 103313.
- 647 42. Selvaraju, G. and N.K.A. Bakar, Production of a new industrially viable green-activated
648 carbon from *Artocarpus integer* fruit processing waste and evaluation of its chemical,
649 morphological and adsorption properties. *Journal of cleaner production*, 2017. 141: p.
650 989-999.
651
652

List of Tables

654 **Table 1.** Newly synthesised green activated carbons (ACs) with raw material and different
655 ratio of the activating agent.

Sample ID	Composition	Mass ratio (sample: KOH)	Activation temperature (°C)
^a NSK1	Walnut shell + potassium	1:1	750
^a NSK2	Walnut shell + potassium	1:2	750
^a NSK3	Walnut shell + potassium	1:3	750
^a NSK4	Walnut shell + potassium	1:4	750
^b PNK1	Peanut shell + potassium	1:1	750
^b PNK2	Peanut shell + potassium	1:2	750
^b PNK3	Peanut shell + potassium	1:3	750
^b PNK4	Peanut shell + potassium	1:4	750
^c PWK1	Pine wood + potassium	1:1	750
^c PWK2	Pine wood + potassium	1:2	750
^c PWK3	Pine wood + potassium	1:3	750
^c PWK4	Pine wood + potassium	1:4	750

656 *** Note: ^aNSK1, walnut shell sample activated with potassium in different m/m ratio; ^bPNK1, peanut shell
657 sample activated with potassium in different m/m ratio; ^cPWK1, pine wood sample activated with potassium in
658 different m/m ratio.
659

Table 2. Chemical analyses of raw biomass material samples.

Biomass samples	Ultimate analysis ^a					Proximate analysis ^c					
	C (%)	H (%)	N (%)	O ^b (%)	S (%)	H/C	O/C	M (%)	VM (%)	FC (%)	Ash (%)
Walnut shell	45.67	6.27	0.40	47.39	0.28	0.14	1.04	7.66	68.56	21.96	1.82
Peanut shell	46.34	6.42	1.95	45.07	0.23	0.14	0.97	6.45	71.87	17.50	4.18
Pine wood	44.78	6.17	0.42	48.38	0.26	0.14	1.08	6.97	72.54	17.07	3.47

661 M, VM, and FC value on dry basis except as denoted in the table.

662 a. Calculated by the difference.

663 b. On dry basis except moisture which is on as received basis.

664 c. As received basis.

665

666

667

Table 3. Surface and pore structure statistics of ACs measured from N₂ sorption.

Sample	S_{BET} (m ² /g)	V_{total} (cm ³ /g)	Average pore diameter (nm)	V_{micro} (cm ³ /g)	$V_{meso} =$ $V_{total} - V_{micro}$ (cm ³ /g)	Microporosity $= V_{micro} / V_{total}$ (%)	Mesoporosity $= V_{meso} / V_{total}$ (%)
PNK3	900.76	0.38	1.69	0.33	0.05	87	13
PNK4	112.33	0.07	2.49	0.04	0.03	57	43
NSK1	603.25	0.22	1.46	0.21	0.01	95	5
NSK3	146.86	0.26	7.08	0.04	0.22	15	85
PWK1	944.05	0.35	1.48	0.33	0.02	94	6
PWK2	581.07	0.29	1.99	0.21	0.08	72	28

668

669

670

671

Table 4. CO₂ uptake rate of synthesised adsorbents.

ACs	Uptake in 1 hour	Uptake in first 120 sec	% CO ₂ uptake in first 120 sec
NSK1	2.71	1.55	57.30
NSK2	2.57	1.35	52.67
NSK3	3.23	1.34	41.64
NSK4	2.90	1.48	50.91
PNK1	3.18	2.80	88.05
PNK2	3.06	2.77	90.38
PNK3	3.92	2.38	60.76
PNK4	2.54	1.04	41.11
PWK1	3.49	3.01	86.21
PWK2	3.24	3.06	94.49
PWK3	2.84	2.00	70.49
PWK4	2.53	1.76	69.66

672

** CO₂ adsorption (over N₂ balance)

673

674

675

Table 5. Production cost estimated for ACs with KOH activation.

676

	Components	US\$/ kg
677	KOH	0.38
678	Distilled water	0.50
679	Nitrogen gas	0.20
680	Power consumption	0.80
681	Transportation	0.05
682	Total	1.93

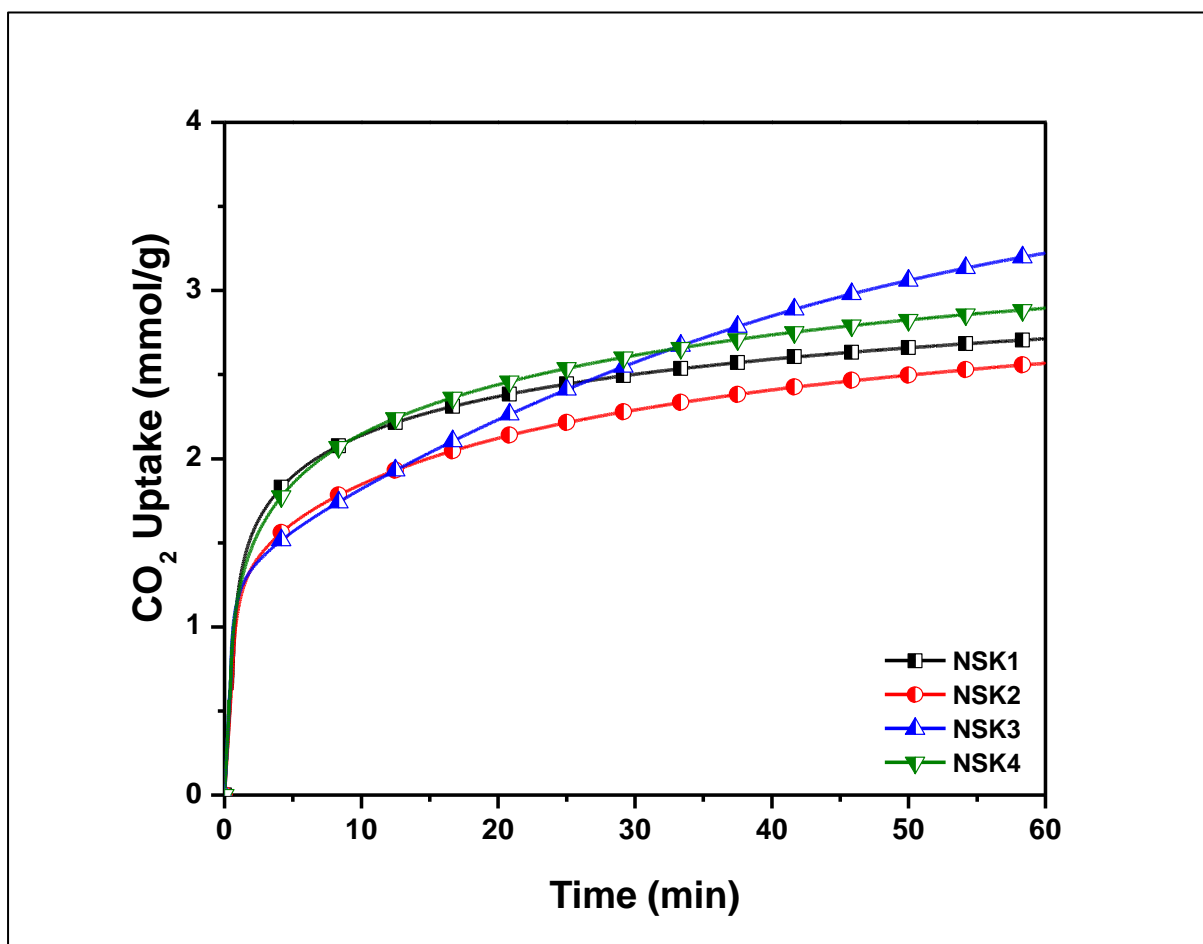
683

684

List of Figures

685

686

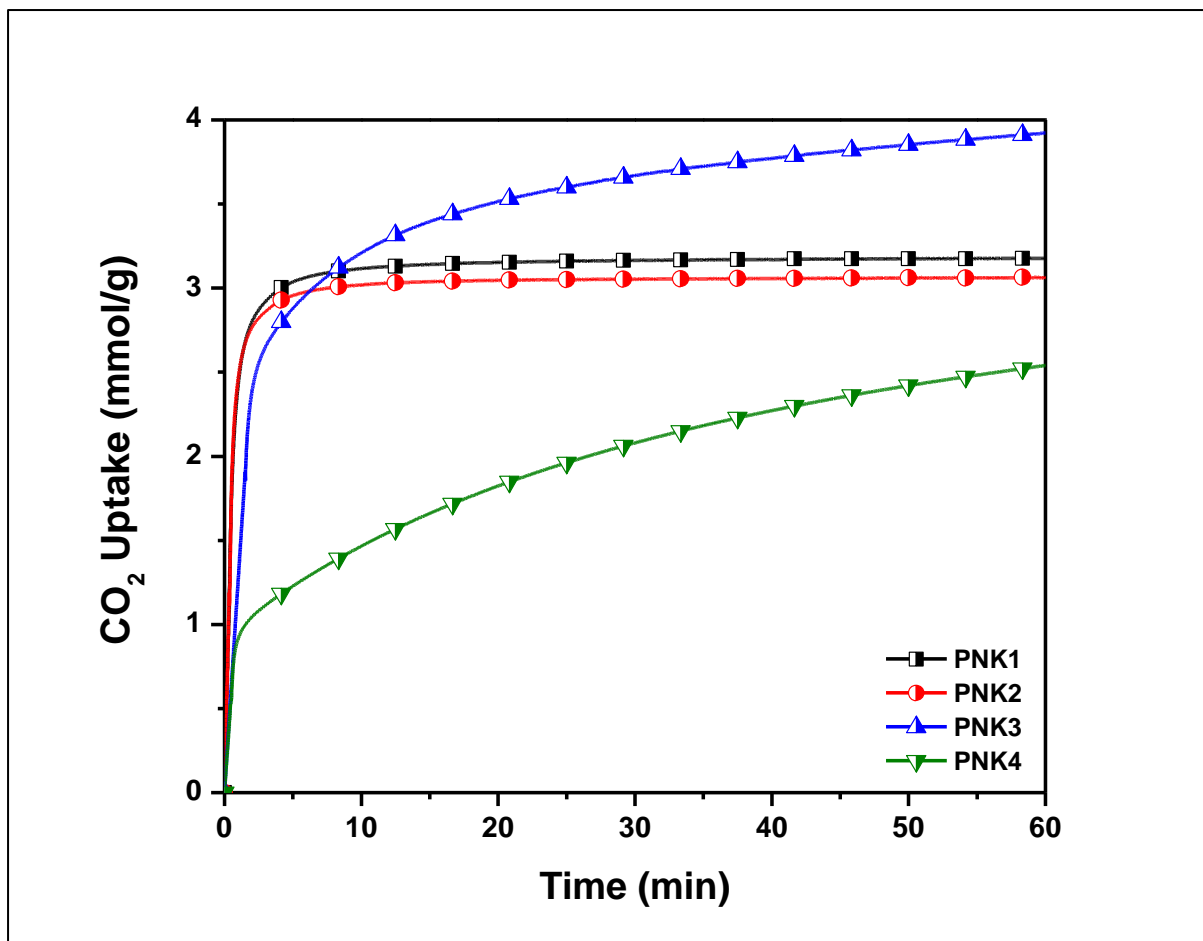


687

688

Fig. 1. CO₂ uptake isotherms of walnut shell (NS) derived ACs at 25 °C.

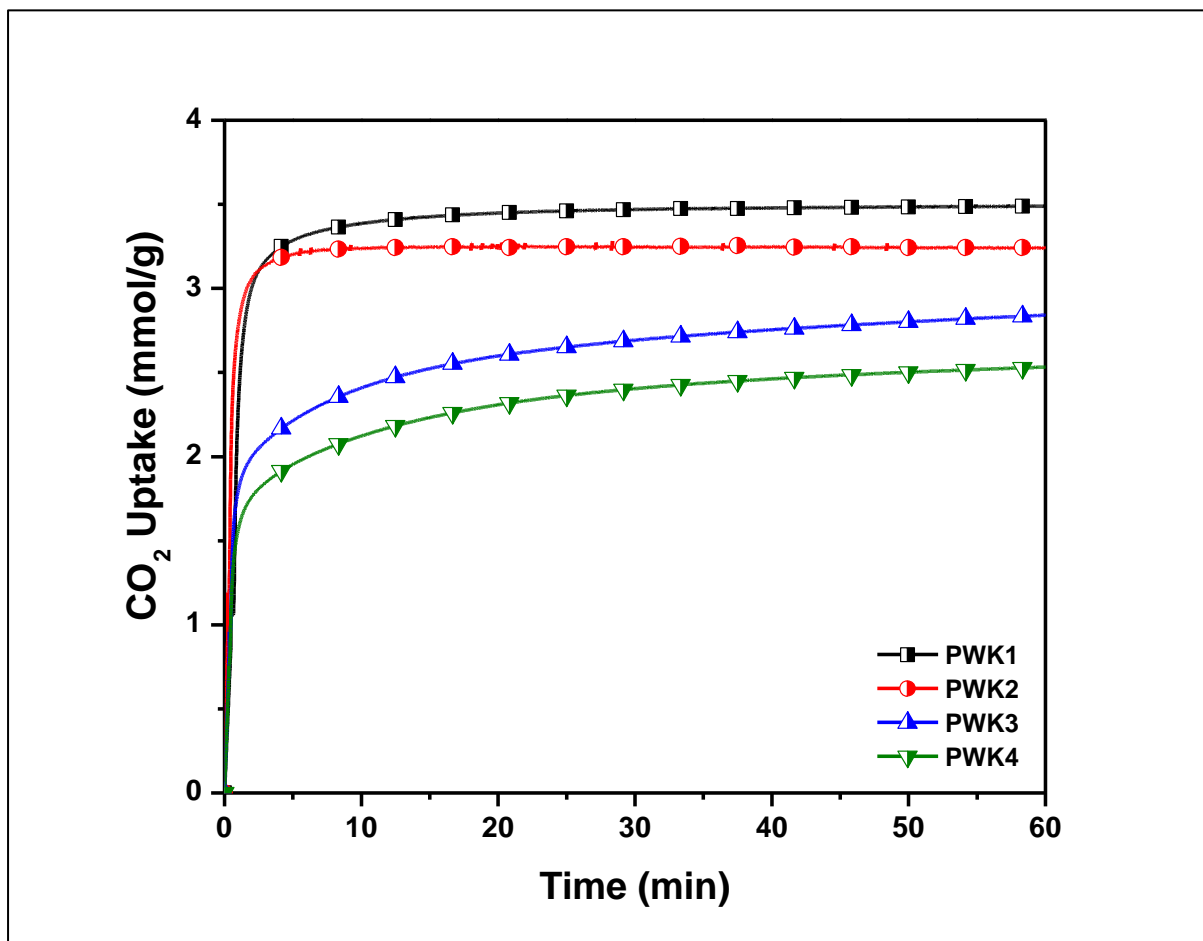
689
690
691
692
693



694
695
696

Fig. 2. CO₂ uptake isotherms of peanut shell (PN) derived ACs at 25 °C.

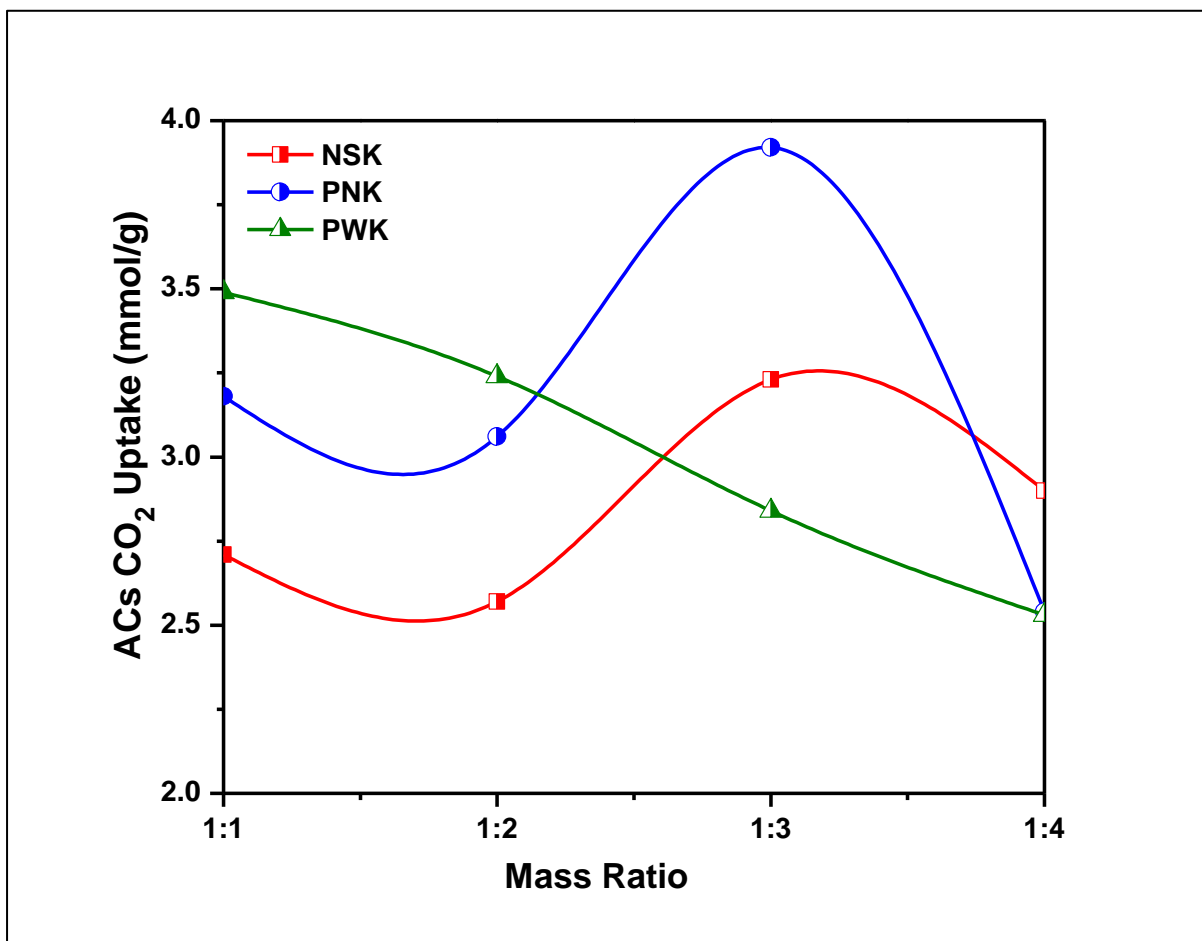
697
698
699
700
701
702
703
704
705



706
707
708

Fig. 3. CO₂ uptake isotherms of pine wood (PW) derived ACs at 25 °C.

709
710
711
712
713
714
715



716
717
718
719

Fig. 4. The role of KOH in CO₂ uptake for adsorbents synthesised from different biomasses.

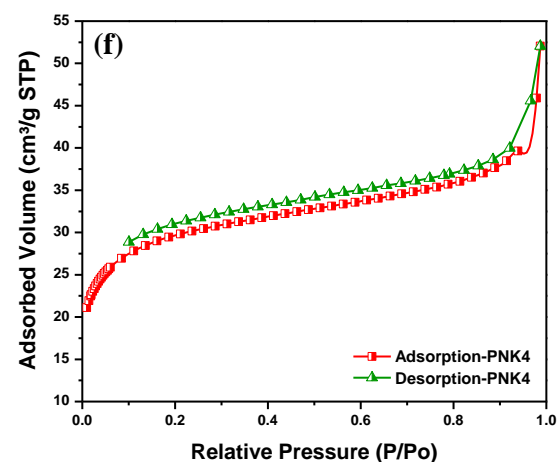
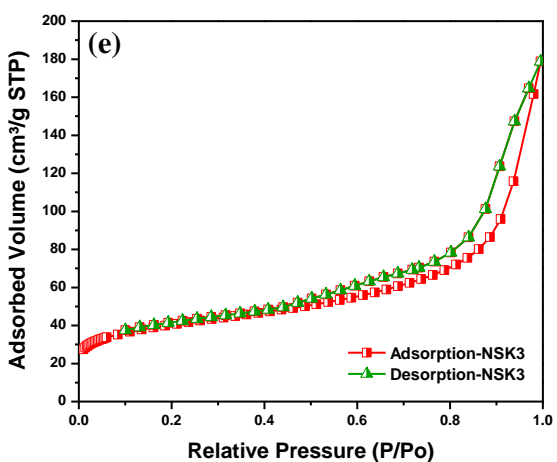
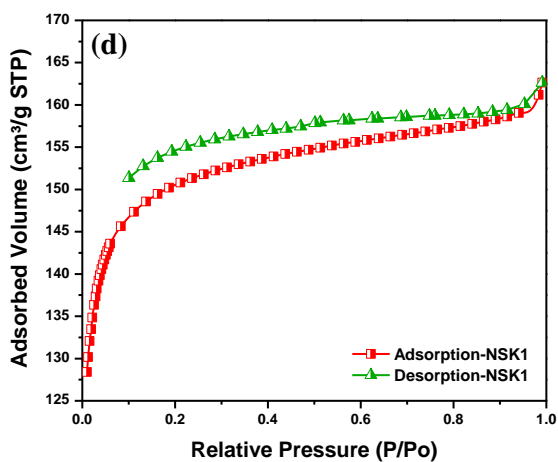
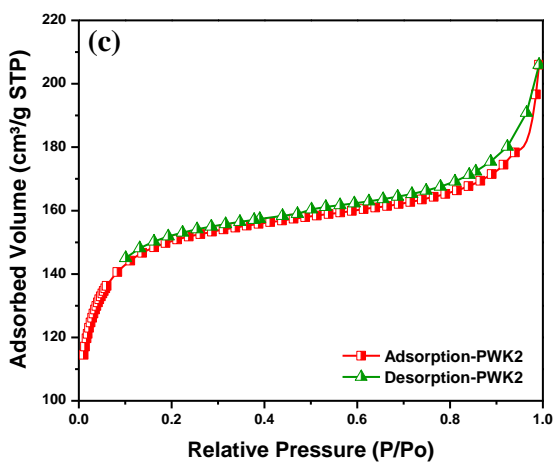
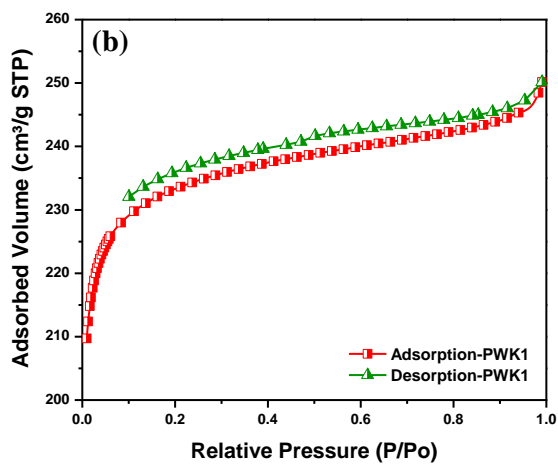
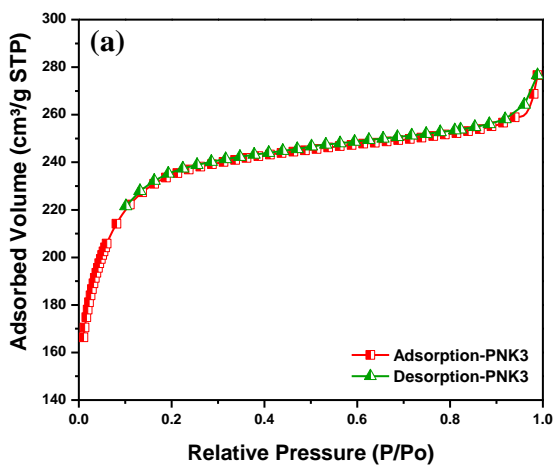


Fig. 5. N₂ adsorptions isotherms of selected ACs; peanut shell group (a and f), pine wood group (b and c) and walnut shell group (d and e).

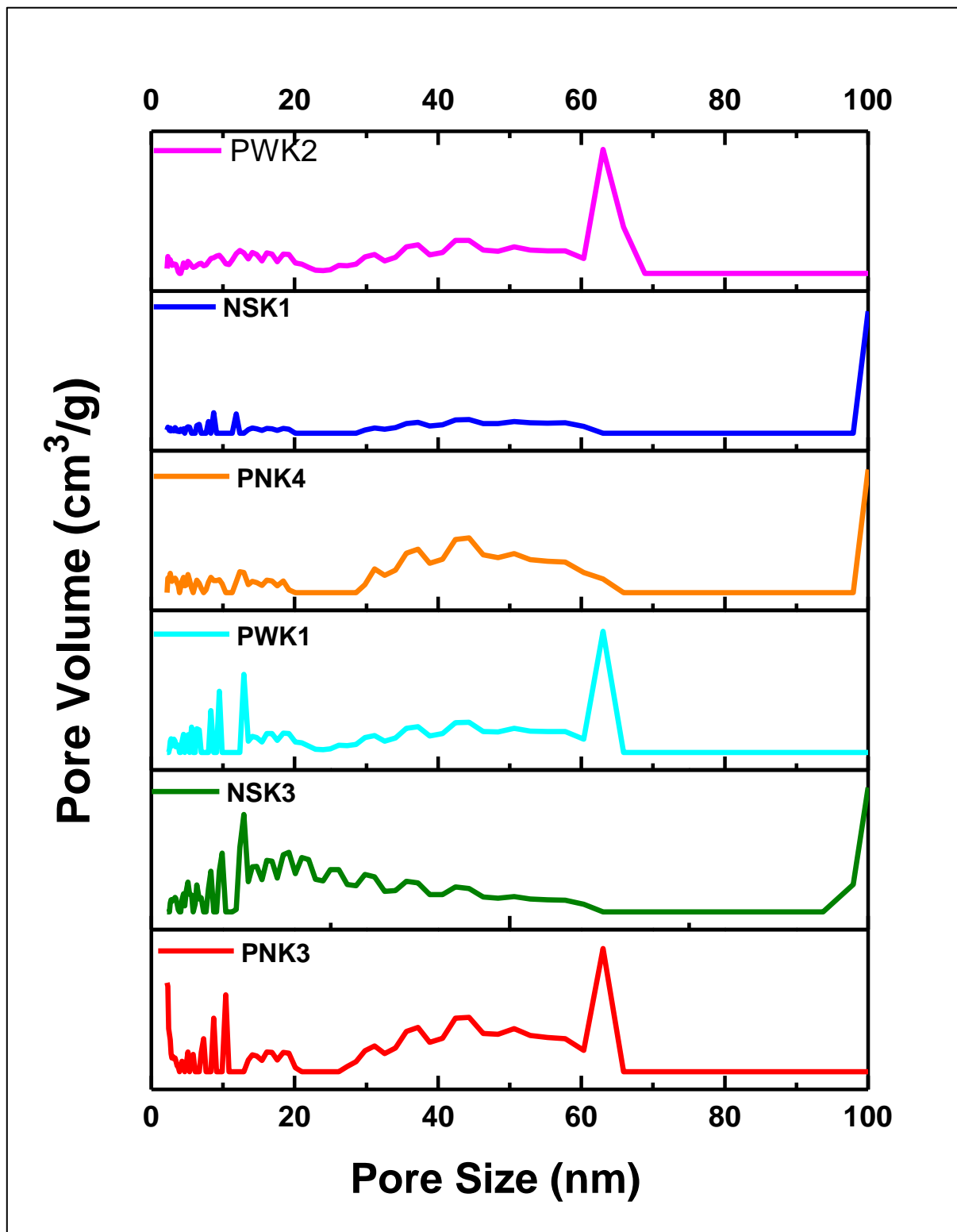
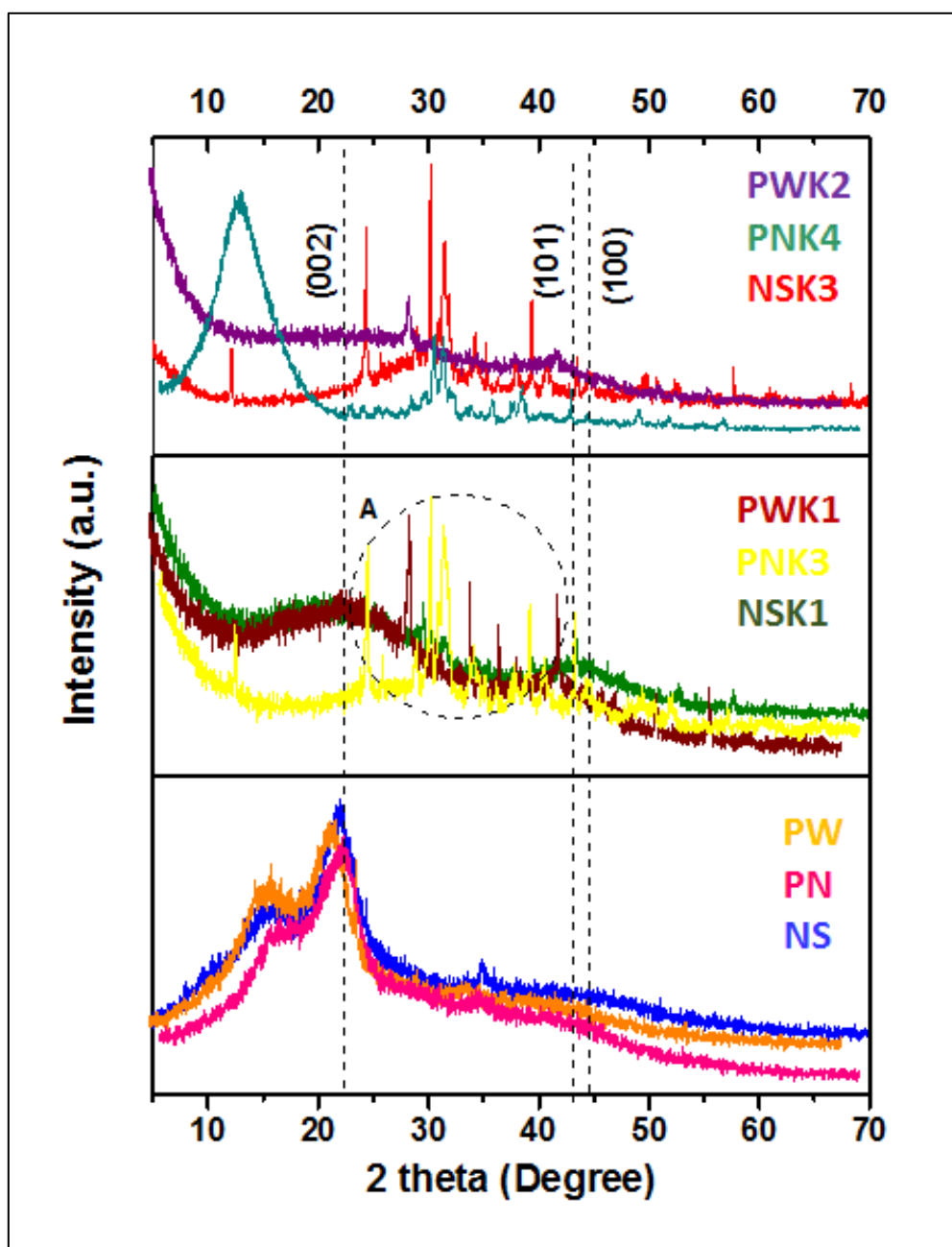


Fig. 6. Pore size distribution for selected samples from different groups of biomass.



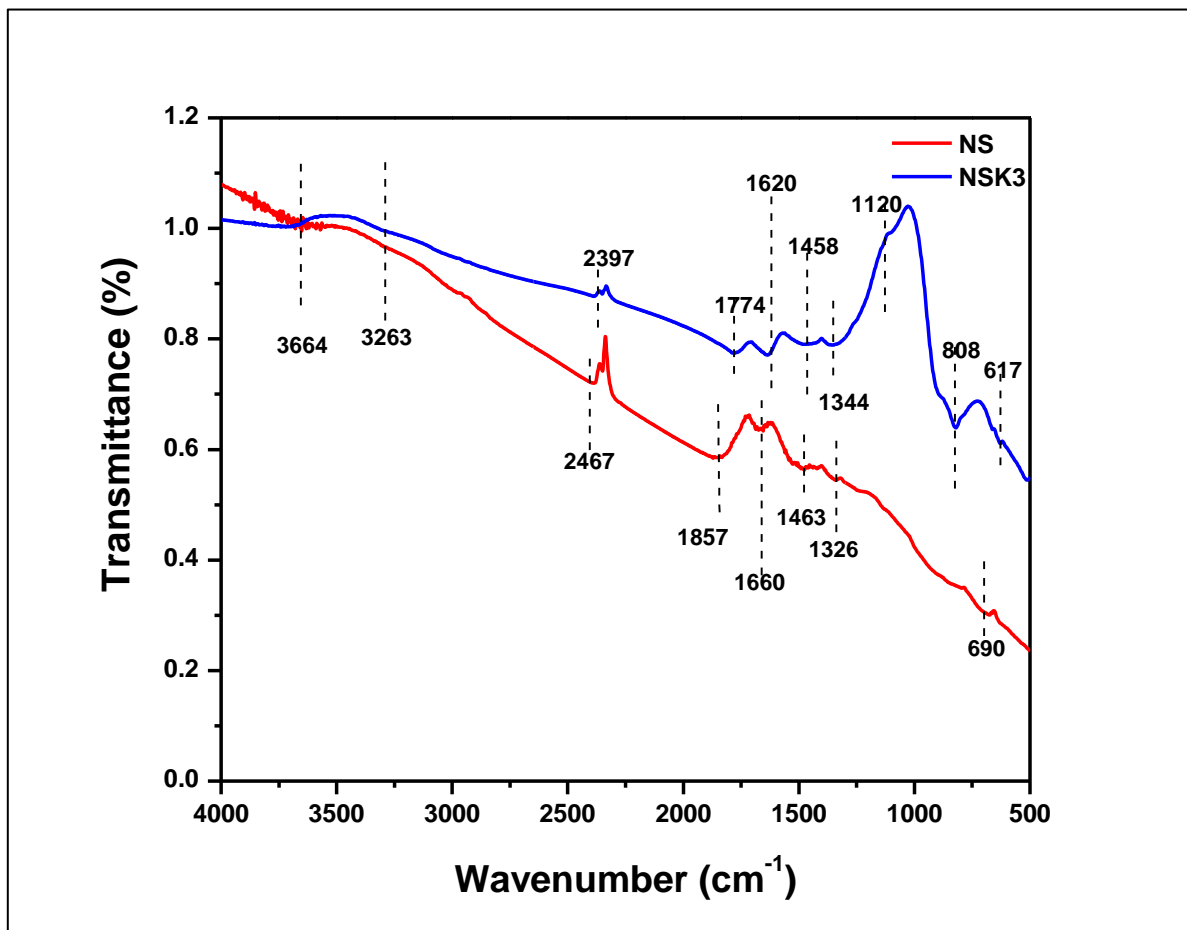
731

732

733 **Fig. 7.** XRD profile of walnut shell, peanut shell and pine wood derived non-activated precursor and activated
734 carbons.

735

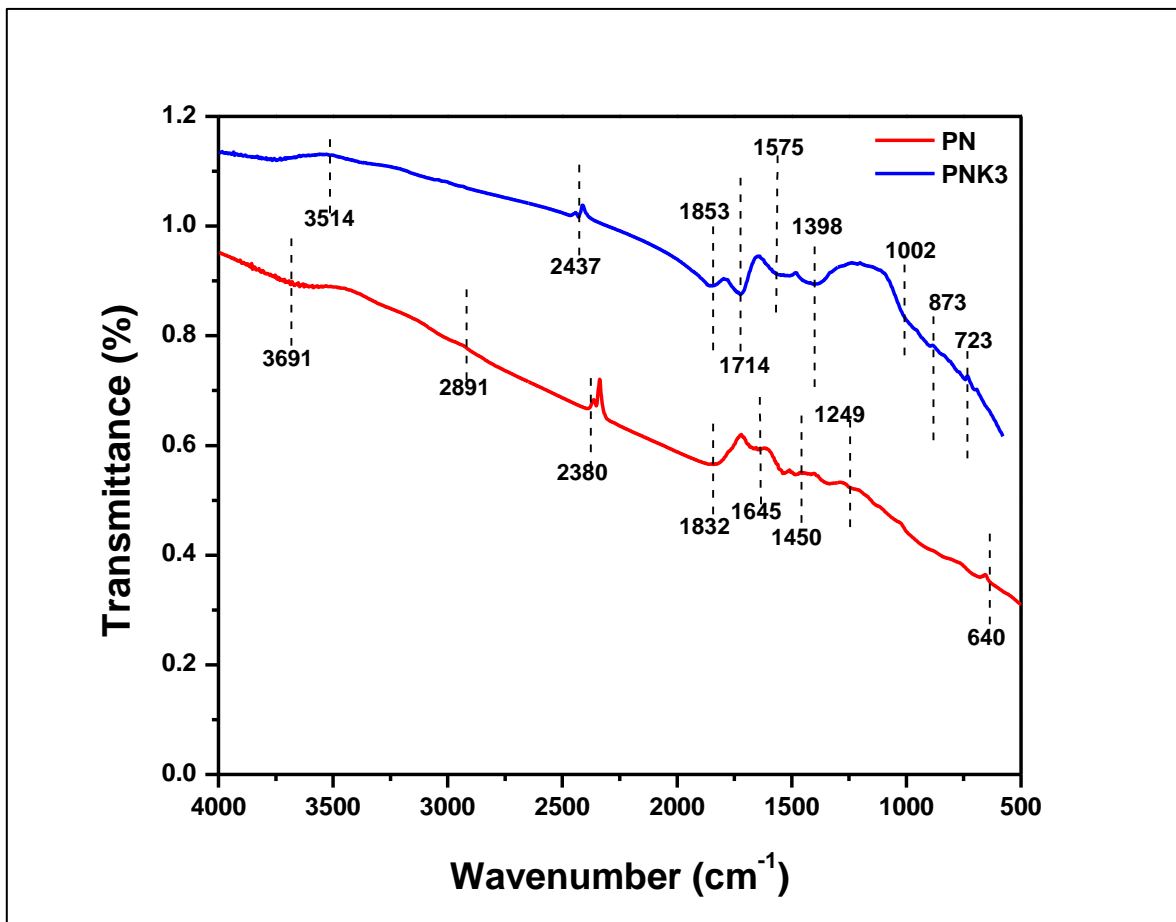
736
737
738
739



740
741
742

Fig. 8. FTIR spectra of walnut shell derived non-activated precursor and activated carbon.

743
744
745



746
747
748

Fig. 9. FTIR spectra of peanut shell derived non-activated precursor and activated carbon.

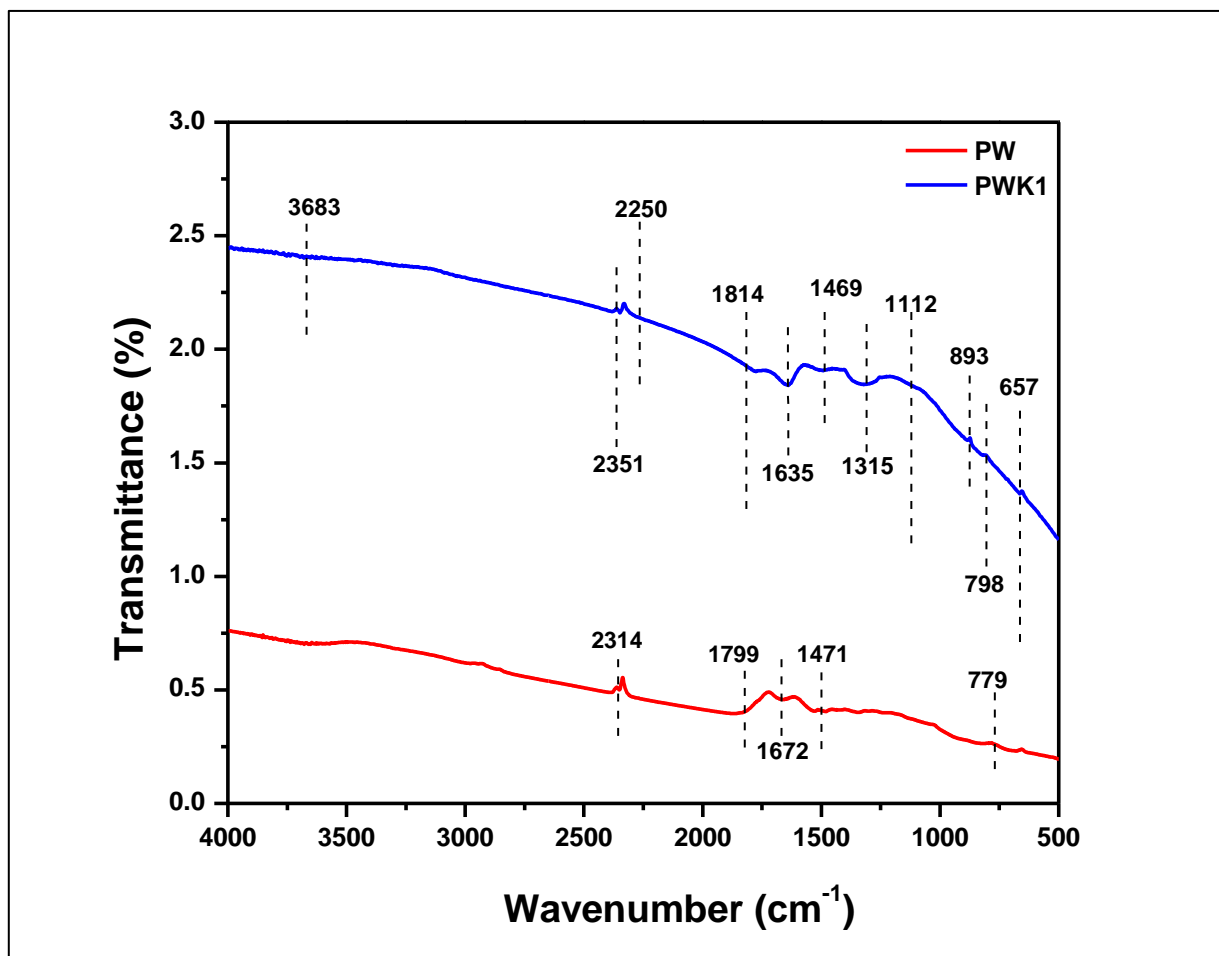


Fig. 10. FTIR spectra of pine wood derived non-activated precursor and activated carbon.

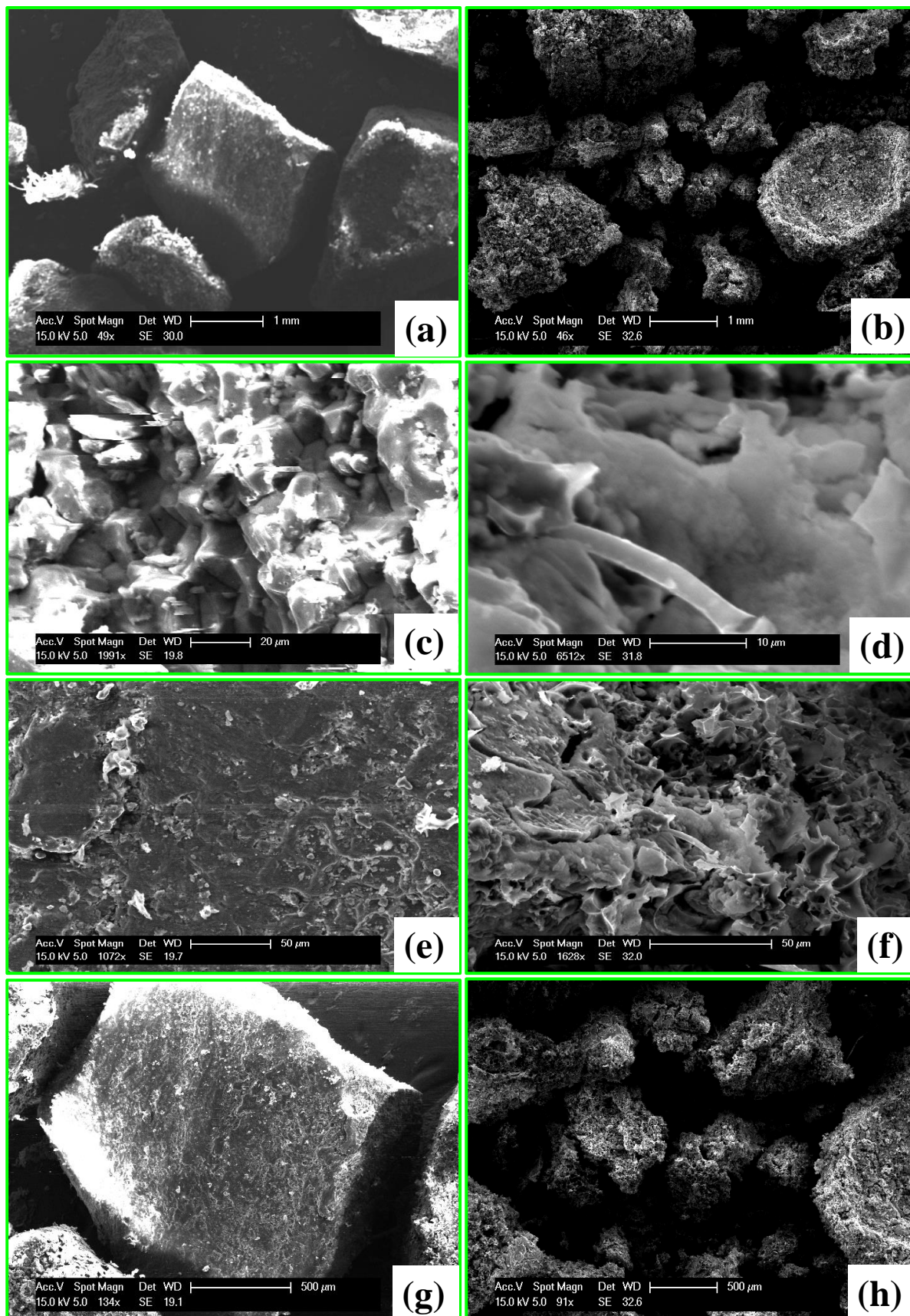


Fig. 11. SEM analysis of walnut shell derived non-activated; NS (a, c, e and g), and activated carbons; NSK3 (b, d, f and h).

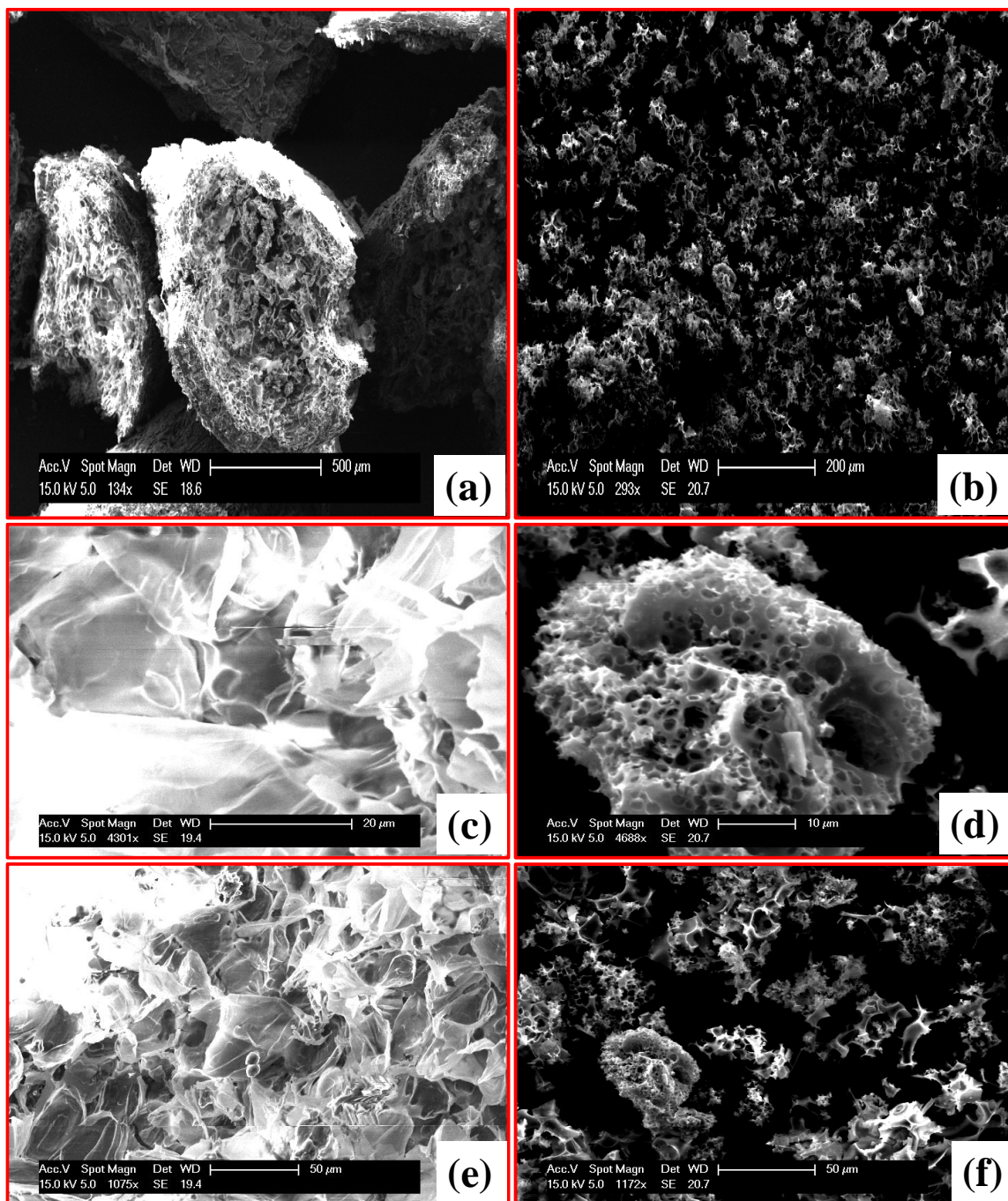
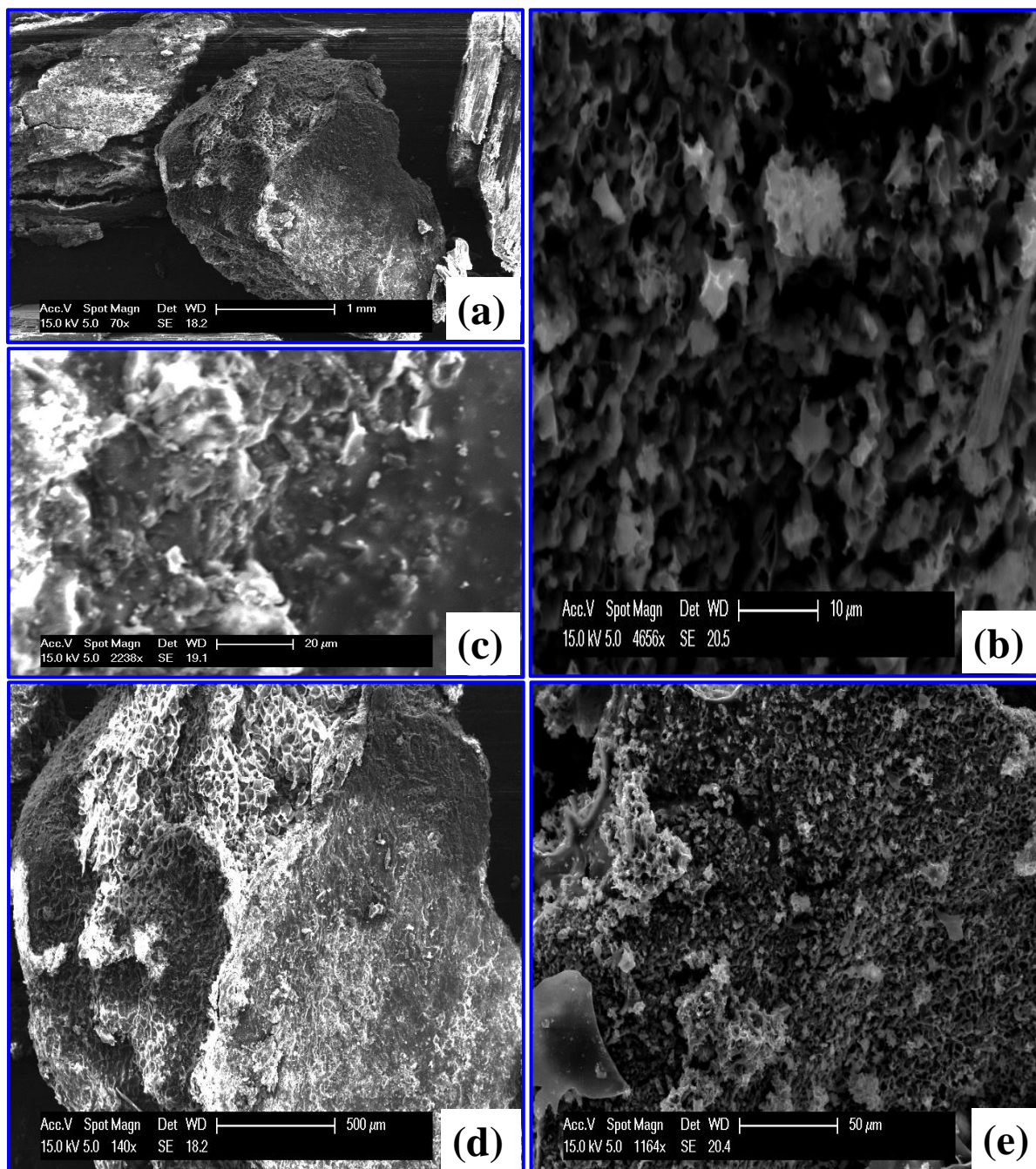


Fig. 12. SEM analysis of peanut shell derived non-activated; PN (a, c and e), and activated carbons; PNK3 (b, d and f).

763

764



765

766

767

768

Fig. 13. SEM analysis of pine wood derived non-activated; PW (a, c and d), and activated carbons; PWK1 (b and e).

769
770
771
772
773
774
775
776
777
778
779
780
781
782
783
784
785
786
787

(Supplementary Material)

Development of biomass derived highly porous superfast adsorbents for post-combustion CO₂ capture

Farooq Sher^{a,*}, Sania Zafar Iqbal^b, Shaima Albazzaz^{c,d}, Usman Ali^e, Daniela Andresa Mortari^f, Tazien Rashid^g

a. School of Mechanical, Aerospace and Automotive Engineering, Faculty of Engineering, Environmental and Computing, Coventry University, Coventry CV1 2JH, UK

b. Department of Biochemistry, University of Agriculture, Faisalabad 38000, Pakistan

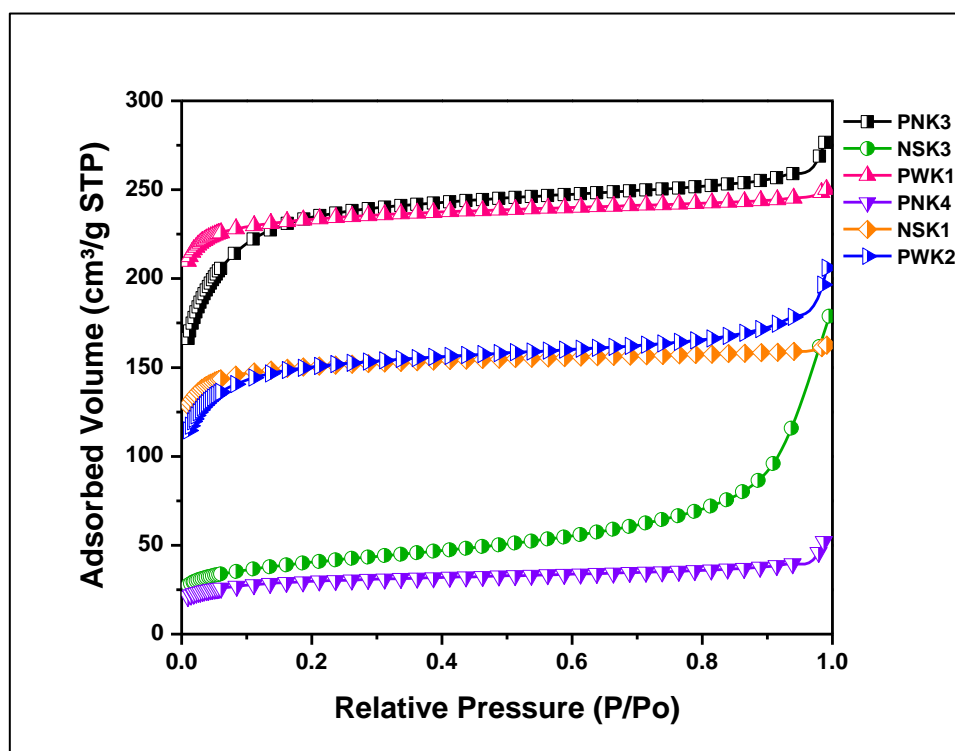
c. Department of Chemical and Environmental Engineering, University of Nottingham, University Park, Nottingham NG7 2RD, UK

d. Department of Chemical Engineering, College of Engineering, University of Basrah, Basrah, Iraq

e. Department of Chemical Engineering, University of Engineering and Technology, Lahore 54890, Pakistan

f. São Carlos School of Engineering, University of São Paulo (USP), São Carlos, SP, Brazil

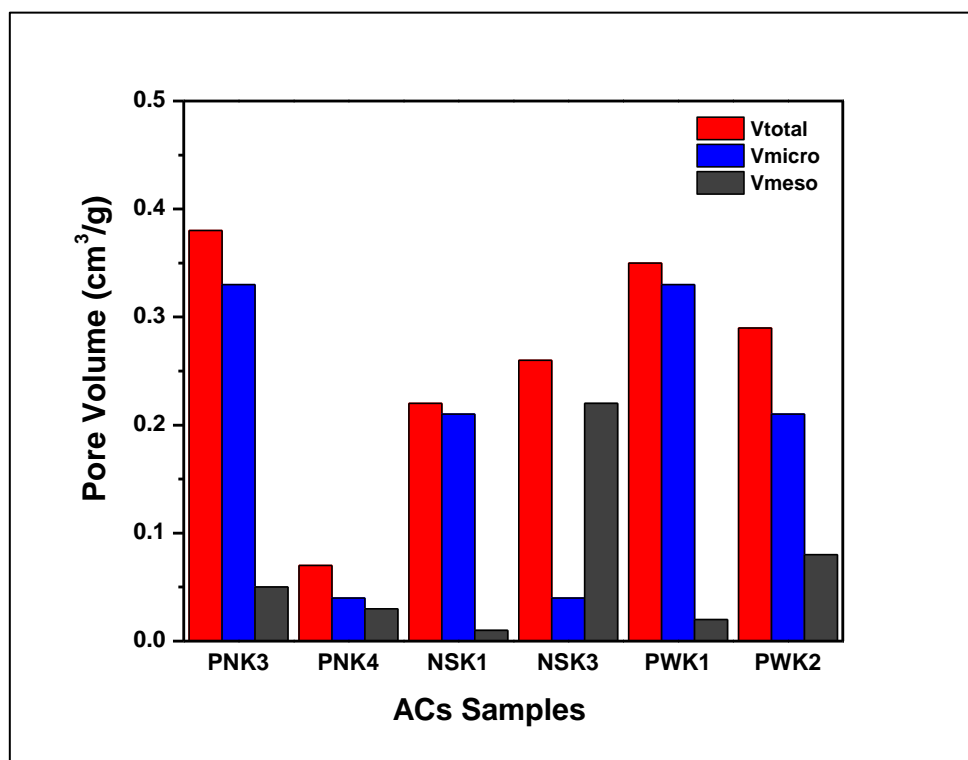
g. Department of Chemical Engineering, Universiti Teknologi Petronas, Bandar Seri Iskandar, Tronoh 32610, Perak, Malaysia



788
789

Fig. S1. Comparison of N₂ adsorption volumes of selected ACs.

790
791
792
793
794
795

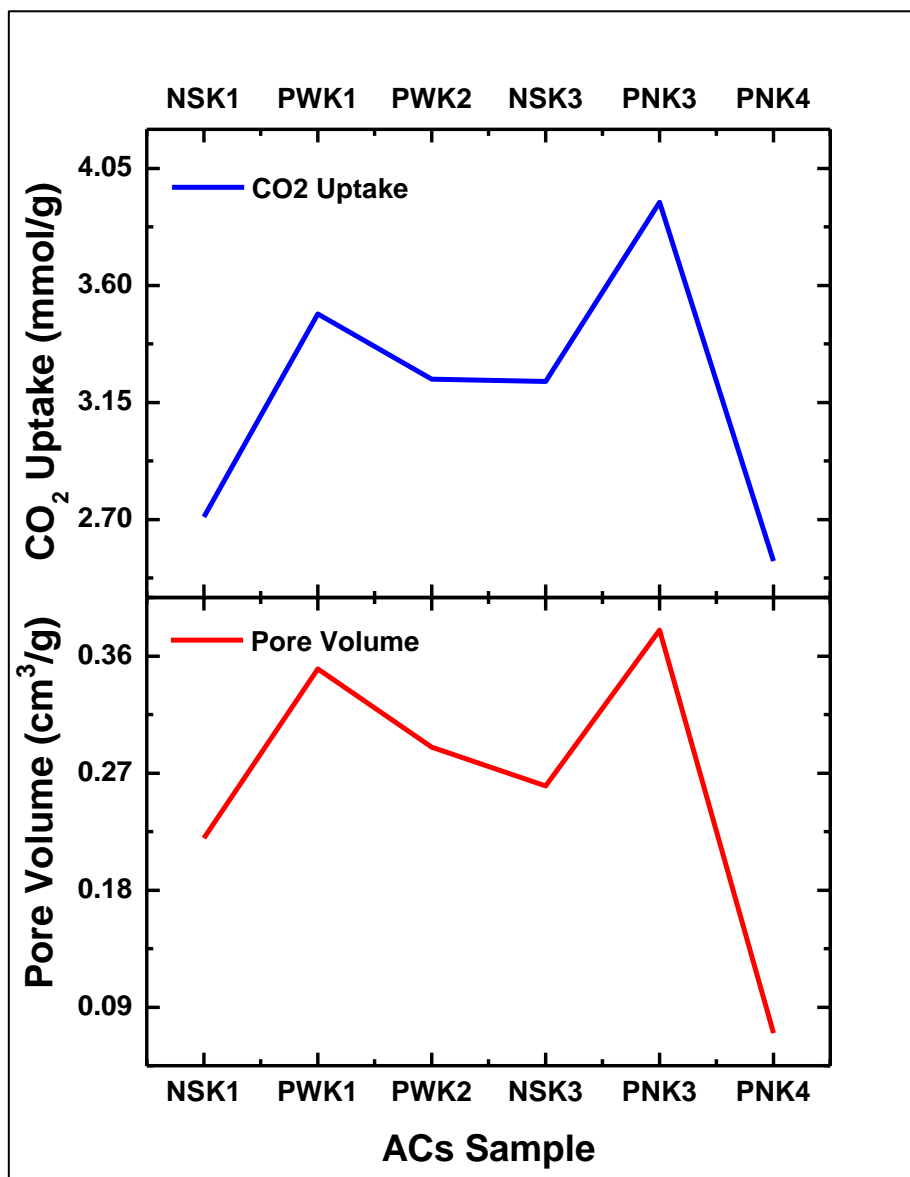


796
797
798

Fig. S2. Comparison of bimodal pore structure of selected ACs.

799

800



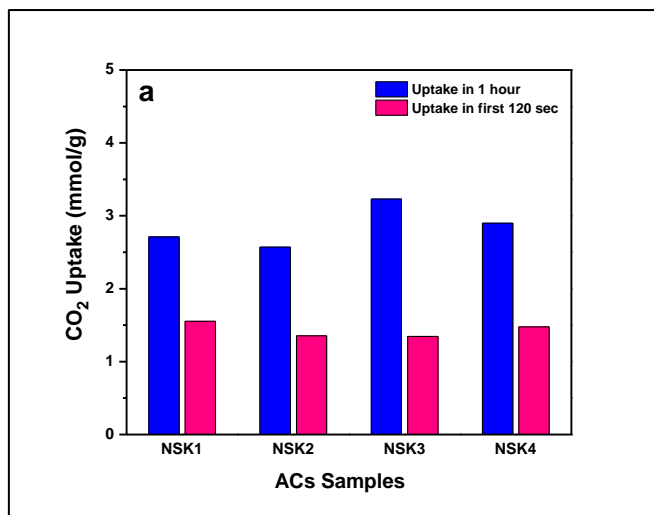
801

802

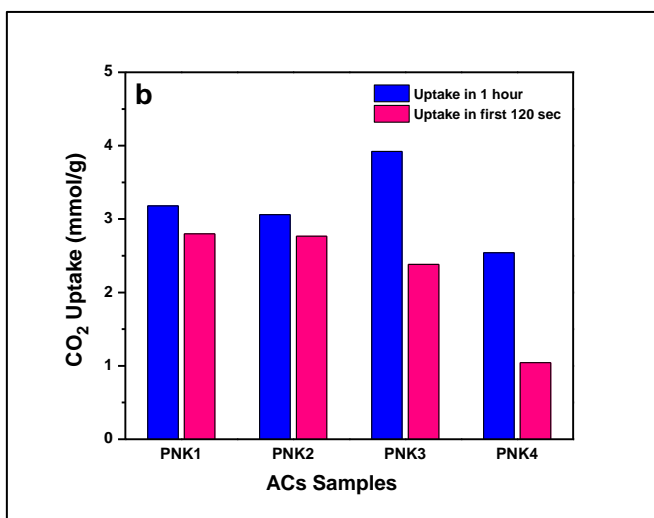
803

Fig. S3. Dependence of adsorbent's CO₂ uptake on pore volume.

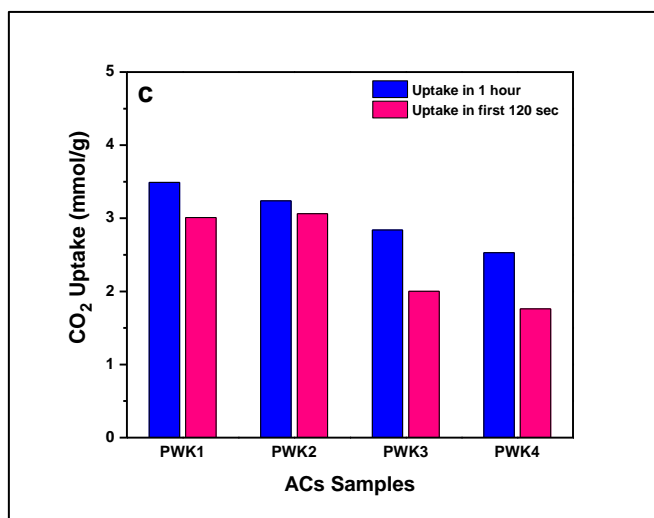
804



805



806



807

808

809

Fig. S4. CO₂ adsorption rate in first 120 sec in comparison with 1 hour; (a) Walnut shell ACs, (b) Peanut shell ACs and (c) Pine wood ACs.